

Article

Towards Balanced Aerodynamic Axle Loading of a Car with Covered Wheels—Inflatable Splitter

Maciej Szudarek ^{1,*}, Konrad Kamieniecki ², Sylwester Tudruj ³ and Janusz Piechna ³

¹ Institute of Metrology and Biomedical Engineering, Faculty of Mechatronics, Warsaw University of Technology, 02-525 Warsaw, Poland

² Institute of Micromechanics and Photonics, Faculty of Mechatronics, Warsaw University of Technology, 02-525 Warsaw, Poland; konrad.kamieniecki@pw.edu.pl

³ Institute of Aeronautics and Applied Mechanics, Faculty of Power and Aeronautical Engineering, Warsaw University of Technology, 00-665 Warsaw, Poland; s.tudruj05@gmail.com (S.T.); janusz.piechna@pw.edu.pl (J.P.)

* Correspondence: maciej.szudarek@pw.edu.pl

Abstract: Generating aerodynamic downforce for the wheels on the front axle of a car is a much more difficult task than for the rear axle. This paper, submitted to the special issue of *Energies* “Future of Road Vehicle Aerodynamics”, presents an unusual solution to increase the aerodynamic downforce of the front axle for cars with covered wheels, with the use of an elastic splitter. The effect of the inflatable splitter on the aerodynamic forces and moments was studied in a DrivAer passenger car and a fast sports car, Arriner Hussarya. Providing that the ground clearance was low enough, the proposed solution was successful in increasing the front axle downforce without a significant increase in drag force. The possibility of emergency application of such a splitter in the configuration of the body rotated by up to 2 degrees with the front end raised was also analyzed. An elastic, deformed splitter remained effective for the nonzero pitch case. The results of the calculations are presented in the form of numerical data of aerodynamic forces, pressure and velocity distributions, and their comparisons. The benefits of the elastic splitter are documented, and the noted disadvantages are discussed.

Keywords: fluid–structure interaction; inflatable splitter; computational fluid dynamics; CFD simulations; aerodynamic downforce



Citation: Szudarek, M.; Kamieniecki, K.; Tudruj, S.; Piechna, J. Towards Balanced Aerodynamic Axle Loading of a Car with Covered Wheels—Inflatable Splitter. *Energies* **2022**, *15*, 5543. <https://doi.org/10.3390/en15155543>

Academic Editor: Antonio Crespo

Received: 2 July 2022

Accepted: 28 July 2022

Published: 30 July 2022

Publisher’s Note: MDPI stays neutral with regard to jurisdictional claims in published maps and institutional affiliations.



Copyright: © 2022 by the authors. Licensee MDPI, Basel, Switzerland. This article is an open access article distributed under the terms and conditions of the Creative Commons Attribution (CC BY) license (<https://creativecommons.org/licenses/by/4.0/>).

1. Introduction

Some racing classes require an uncovered wheel design. For various reasons, most other cars have covered wheels. Among others, uncovered wheels are the strongest source of aerodynamic drag. Therefore, for aerodynamic reasons, cars typically use fenders hiding the wheels or have their wheels completely covered. Hiding the wheels in the body contour, on the one hand, lowers its aerodynamic resistance and, on the other hand, makes it difficult to shape it in such a way as to obtain the necessary aerodynamic downforce of the front axle.

The car’s directional stability depends on the relationship between the front and rear axle drift angles. Larger drift angles of the front axle than the rear axle make the car directionally stable. As the drift angles depend mainly on the wheel vertical load, the downforce of the front wheels should generally be greater than that of the rear wheels. The aerodynamic forces, and also the downforce, depend on the speed squared. Depending on the driver’s preference, the car can be set to oversteer, neutral, or understeer [1]. It seems that a car with neutral or slightly understeer characteristics gives drivers more room for maneuver. Operating the torque transferred to the rear axle wheels makes it possible to change the directional characteristics of the car to oversteer. Therefore, the body of the car and its additional elements should be shaped in such a way that the directional characteristics of the car do not change significantly with the change in the driving speed.

Consequently, the aerodynamic loads on the front axle should be slightly smaller than on the rear axle within the whole range of usable speeds.

This is how it looks from the point of view of directional stability. However, there is also a problem of longitudinal stability [2]. The aerodynamic characteristics of the body and the additional elements placed on it depend on the angle of the body in relation to the road as well as the distance of the body from the road. Wheel suspensions must be flexible and the body usually oscillates about the body's transverse axis, changing the distance of the front and rear of the body from the road. Typically, lifting the front end causes the aerodynamic downforce of the front axle wheels to decrease. The same occurs when driving over hilltops or when the body enters the aerodynamic wake of the preceding car.

Designers of cars with covered wheels have no problem providing significant aerodynamic downforce to the car's rear axle; see [3–8]. Using inverted wings and diffusers in the rear of the body is a typical solution for aerodynamic downforce of the rear wheels [9]. While aerodynamic downforce for the rear wheels can be realized with a relatively small increase in aerodynamic drag, generating aerodynamic downforce for the front wheels of a car with covered wheels has always been a problem. In the body's front part, a range of solutions is used: slanted inverted wings (canards), splitters, air dams, and local diffusers [10]. The aerodynamic characteristics of aerodynamic elements alone do not reflect their actual properties when mounted on a car body. This is especially true for aerodynamic elements designed to operate at the front of the body. The elements themselves generate aerodynamic forces, but these are compensated for by changes in the body flow structures behind them. In summary, generating vertical forces at the front end of a vehicle is difficult, as indicated in [11,12]. The use of flat undersides and flat splitters makes them extremely sensitive to the amount of underbody clearance. Additionally, the stiffness of the front and rear suspension affects the angular position of the body with respect to the roadway.

The importance of the aerodynamic downforce of the front wheels is highlighted by a number of spectacular accidents that occurred on race tracks over the years. For example, in 1999, when a vehicle followed its predecessor [13], or when climbing a hill [14], causing aerodynamic components in the front of the body to stop working. Analysis of aerodynamic force changes in a much wider range of pitch angles was performed in [15]. There is a film [16] presenting the causes and course of the accident of Yannick Dalmas in a Porsche GT1 in Road Atlanta very precisely. The driver of the Porsche, being in the aerodynamic wake of its predecessor, accelerated too rapidly, causing a loss of downforce on the front axle and ending in a loop in the air and a lucky landing partly on wheels. Even in the case of such a tragic accident as the 1955 Le Mans crash, caused by a collision between two cars, the possible influence of aerodynamic elements on the accident is sought [17].

This issue was addressed by several researchers. In [18], the solution of a lowered rounded spoiler located under the front bumper of the Mitsubishi 3000 GT and its effect on the generation of the car's lifting force is presented. In [19], it is presented that a deployable front spoiler with a rounded valance leading edge surface was incorporated in the construction of the Ford Probe IV. A more modern solution in the form of the profile deployed at high speed is presented in [20], and in [21] a movable spoiler or air dam is deployed by a pneumatic actuator. In [22], the aerodynamic performance of a car at different overhang lengths of a splitter attached to the body of a 2019 NASCAR model is analyzed using computational fluid dynamics (CFD). In [23], a methodology for obtaining various performance modes, such as oversteer, understeer, minimum drag, or maximum downforce is shown, with the use of active aerodynamics including an active splitter. In [24], transient aerodynamic characteristics were studied for a pitching motion.

This study aimed to test the aerodynamic properties of a slightly different solution. A concept of an elastic bottom surface located under a rigid splitter base that expands toward the roadway under the influence of air delivered over it at a specified pressure is presented.

There are known solutions called hidden wings, as in the case of Toyota [2]. They have the form of convex cylindrical surfaces. The analyzed solution of the inflatable splitter is

similar, except that the curvature of the bottom surface of the splitter is three-dimensional instead of two-dimensional.

The proposed and analyzed inflatable splitter system is somewhat similar to that studied in the Mercedes 500 ESF 2009 Experimental Safety Vehicle [25]. This is a system utilizing a special airbag equipped with friction surfaces, mounted under the front of the car's body. PRE-CRASH sensors installed in Mercedes-Benz cars are able to initiate preventive measures to protect passengers in critical driving situations. If the sensor system determines that an impact is imminent, the PRE-SAFE[®] system not only initiates automatic emergency braking but also deploys a braking airbag. Thanks to the car body's vertical inertia and a friction coating, the airbag supports the car against the road surface, shortening the braking distance. The braking airbag also gives the effect of an additional crumple zone—Mercedes engineers have calculated that even at a low speed of 50 km/h, the additional braking has the same effect as extending the front by 180 mm. However, this braking airbag is built differently and is designed to implement a different physical process.

The concept of a flexible inflatable splitter is studied in this paper with the use of computational fluid dynamics (CFD) and mechanical analyses. First, the methodology of the performed two-way fluid–structure simulation is described. As a preliminary analysis, the already deformed elastic splitter was mounted on a DrivAer passenger car body and compared with solutions without or with a rigid splitter. As a continuation of the work carried out on passenger cars, the elastic splitter was then mounted on the sports car Arrinera Hussarya. The study on Arrinera Hussarya was extended by the verification of the performance of the elastic splitter for pitch angles up to two degrees.

This paper is a small contribution to the solution of the problem of balanced aerodynamic axle loading of a car with covered wheels. The goal is to improve downforce on the front axle and improve safety (countering the pitching moment). The context is both sports cars and passenger cars, hence the analyses for the DrivAer and Arrinera Hussarya cases. The obtained results are also compared in Appendix A against the existing data of Mercedes LMP-class cars [14].

2. Materials and Methods

2.1. CFD Models

2.1.1. Passenger Car

In the past, many numerical analyses in the field of vehicle aerodynamics were carried out on highly simplified models such as Ahmed's body, or on models of real vehicles freely chosen by the authors. In the latter case, due to different geometries, it was difficult to compare the obtained results. In order to solve this problem, a generally available realistic car model (DrivAer body) was developed. Several types of bodywork are available to download [26]. For the purpose of this analysis, a fastback configuration was selected, which is shown in Figure 1.

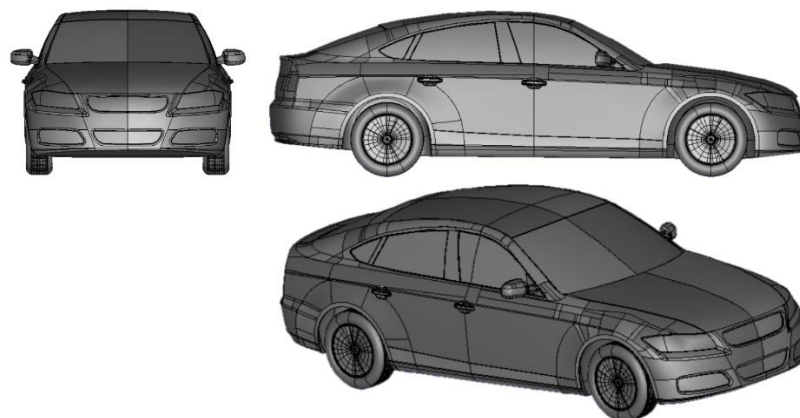


Figure 1. DrivAer model in the fastback configuration.

The analysis of a DrivAer car was performed for a symmetric half of the model. The domain size is shown in Figure 2.

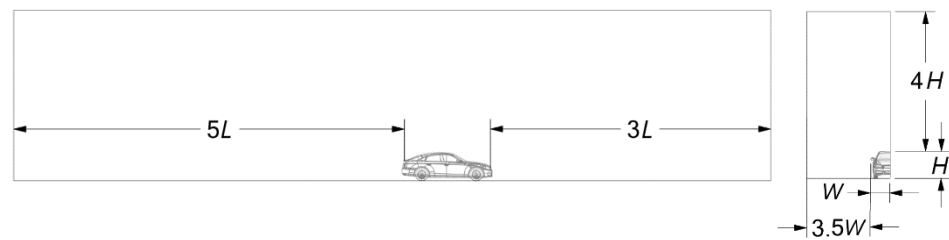
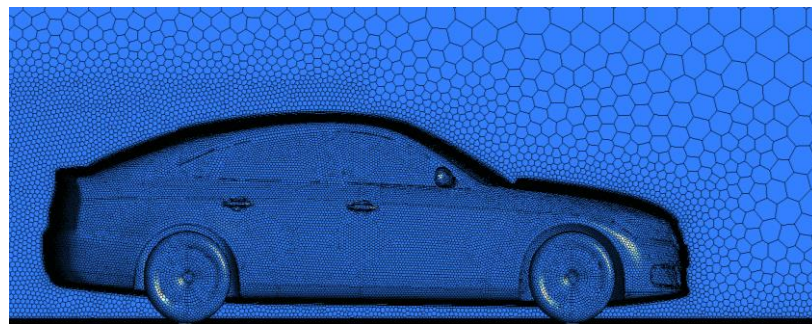
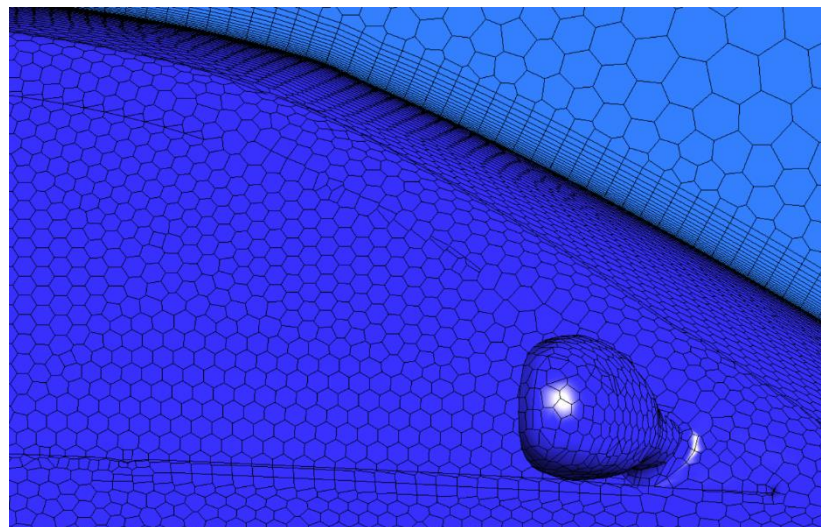


Figure 2. Computational domain for the DrivAer case, with length $L = 4.6$ m, height $H = 1.4$ m, and width $W = 1$ m.

A polyhedral mesh was created in Fluent Meshing 2021R1. A boundary layer consisting of 15 layers with a growth rate of 1.2 was generated for the wall function approach, as shown in Figure 3a,b.



(a)



(b)

Figure 3. Mesh for the DrivAer case: (a) side view of the car; (b) zoomed in view of the boundary layer mesh.

The inlet velocity was set to 40 m/s with 2% turbulent intensity and a turbulent length scale of 0.04 m. Considering the length of the vehicle, this corresponds to a Reynolds number of ca. 12×10^6 . The rotational velocity of the wheels was taken into account by means of a moving wall boundary condition. The ground was treated as a moving wall. The side and top faces had a symmetry boundary condition. The k- Ω BSL turbulence model has been chosen, taking into account suggestions presented in [27].

A mesh sensitivity test was carried out. For this purpose, five simulations were performed for meshes with cell counts ranging from 675,000 to 2.8 million. A mesh with a cell number of 2.2 million was selected as the target and, as for denser mesh, the aerodynamic force coefficients did not change by more than 0.003. Results are shown in Figure 4.

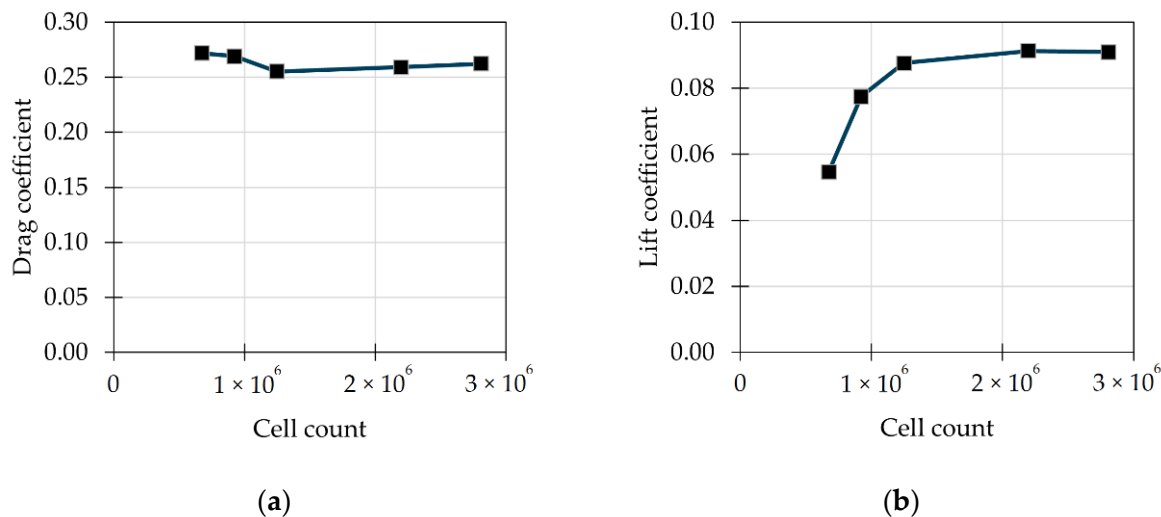


Figure 4. Mesh convergence test: (a) drag coefficient; (b) lift coefficient.

Iterative calculations were performed with a coupled pseudo-transient scheme. If oscillations were present, then iterative calculations were run until 10 periods of stable oscillations were captured and the mean value was taken as a result. Consequently, when pressure and velocity contours or plots are reported, they are averaged fields from a number of periodic oscillations.

Lift and drag coefficients C_L and C_D are nondimensionalized by the reference values of inlet velocity, the density of 1.225 kg/m^3 , and the area of 1.102 m^2 which corresponds to the projected front area of a symmetric half of the car. The pitching moment was computed along an axis placed in the middle of the distance between car axles. The moment coefficient C_M was nondimensionalized by the distance between the axles, which was equal to 2.794 m . A positive moment coefficient indicates dominating downforce on the front axle.

To confirm the correctness of the constructed model, the results obtained for the basic configuration of the car, without additional aerodynamic elements, were compared with the results of simulations and experiments available in the literature. The comparison is shown in Table 1. It confirmed the validity of the assumptions made during the construction of the model.

Table 1. Comparison of drag coefficients between the simulation and experimental data from [24].

	Experiment	Simulation, k-Omega SST	This Work, Simulation k-Omega BSL
Drag coefficient	0.254	0.260	0.259

2.1.2. Sports Car

The CFD mesh for the sports car consisted of around 12 million cells generated with the hexcore algorithm. Based on our knowledge and good practices [28], the boundary layer had five prism cells on the car body generated for the wall function approach. Boundary conditions were set in the same way as for the DrivAer case, and the realizable k-epsilon turbulence model was used. The grid convergence test, together with validation of the numerical model of Arrinera Hussarya, were reported by the authors of [29], where compliances of drag coefficient and lift coefficient of 3.8% and 6.5% were obtained, respectively. The inlet velocity was set to 40 m/s with 2% turbulent intensity and a turbulent length

scale of 0.04 m. The rotational velocity of the wheels was taken into account by means of a moving wall boundary condition. The ground was treated as a moving wall. The side and top faces had a symmetry boundary condition. Domain extent is shown in Figure 5a, and mesh is shown in Figure 5b,c.

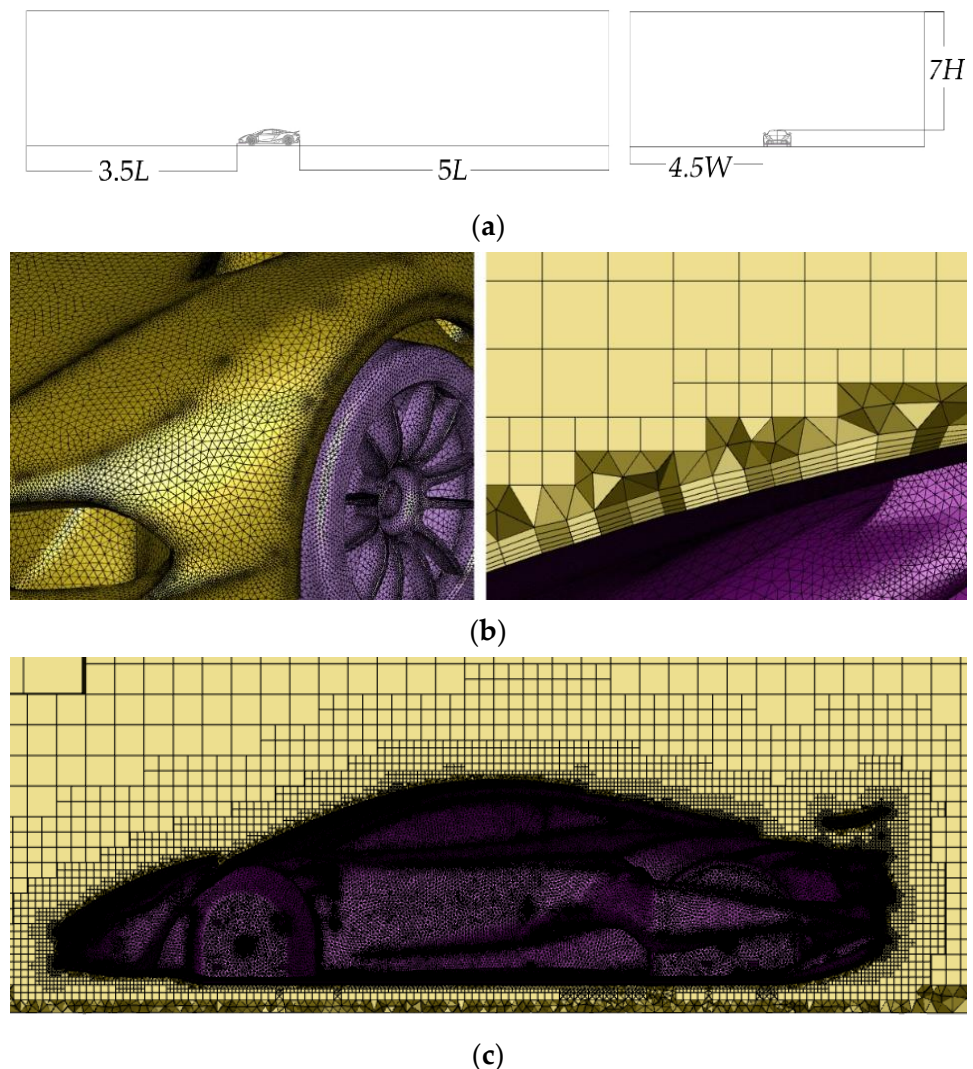


Figure 5. CFD computational domain for the Arrinera Hussarya case: (a) domain extents with length $L = 4.6$ m height $H = 1.1$ m, and width $W = 2.2$ m; (b) surface mesh and zoomed in view of the boundary layer; (c) a cross-section of the volume mesh.

2.2. Flexible Splitter Model

To obtain a better balance between downforce generated on the front and rear axles, an elastic inflatable splitter was proposed. The solution shown in Figure 6 uses a flexible bottom surface located under the rigid base of the splitter, which expands toward the roadway due to the applied pressure. The deformation of the bottom elastic shell takes place because of the pressure difference between its interior and exterior. To be able to calculate the elastic deformation of the splitter, the fluid–structure interaction technique was employed.

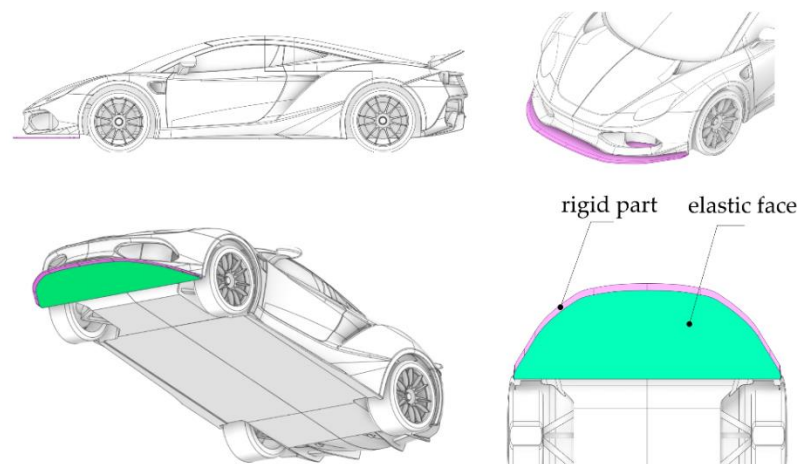


Figure 6. Elastic splitter mounted on the Arrinera Hussarya car body.

Structural and fluid domains were solved in steady state using ANSYS Mechanical and ANSYS Fluent solvers, respectively. The coupling is presented schematically in Figure 7. Data exchange was carried out only on the splitter's flexible face. The pressure distribution on the car with the splitter calculated in ANSYS Fluent was used as a boundary condition for the splitter structural model. The splitter deformed due to the pressure difference between the interior and the exterior faces. The geometry of the deformed splitter face was sent back to the Fluent software, which forced Fluent to generate a new mesh and obtain a new flow field. Thirty mechanical solver iterations were calculated per single fluid iteration. The iterations between solvers were repeated several times to achieve a balance between the pressure distribution and the deformation of the elastic shell.

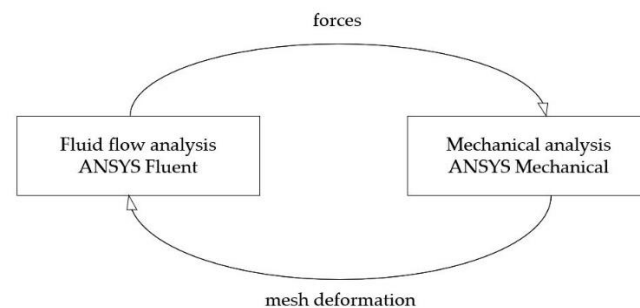


Figure 7. Data transfer scheme in steady-state fluid–structure interaction simulation.

Since 2003, the authors have been involved in simulations of airbag deployment based on a proprietary validated code developed using a lumped parameter model of an airbag shell in a compressible air environment [30–32]. The effect of air inertia in front of a fast-moving gasbag shell was taken into account. In the current paper, due to the complicated external zone around the flexible splitter surface strongly influenced by its shape, professional software was chosen for simulations.

The structural model consisted only of the flexible face of the splitter. It was modeled as a membrane, without taking into account the bending stiffness. Its thickness was equal to 5 mm. As the thickness of the membrane was at least one order of magnitude lower than the two remaining dimensions, the splitter was modeled as a shell body. It was meshed using triangle SHELL181 finite elements of a size equal to 2.5 cm. The mesh consisted of 1617 nodes and 3044 elements. The linear material model of Young's moduli $E = 10$ MPa and Poisson ratio $\nu = 0.49$ was used [33]. Linear mechanical properties can be assumed for rubbers working in a small deformation range. Translations of the edges of the elastic splitter's face were restrained. The pressure distribution calculated in Fluent was applied

to the outer face of the splitter. A constant pressure of 1000 Pa was applied to the inner splitter's face.

3. Results

3.1. Inflatable Splitter

The pressure distributions on inflated and flat splitters which were calculated in ANSYS Fluent are presented in Figure 8. Due to convexity, the larger suction pressure is obtained in the case of an inflated splitter. This effect will be used to increase the downforce acting on the front axle. Due to a nonperfectly symmetric mesh, some asymmetries are observable in the contour plots.

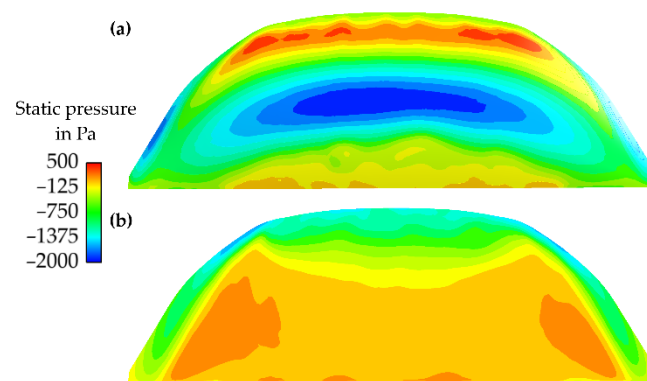


Figure 8. Comparison of pressure distributions from a CFD simulation: (a) inflated splitter; (b) flat splitter.

Due to the generated pressure difference, the splitter's maximum deflection was approximately 6.5 cm. The deformation is presented in Figure 9. The spatial dimensions of the splitter are approximately $0.65 \text{ m} \times 1.9 \text{ m}$. Thus, the deformation of 6.5 cm was recognized as small compared to the outer dimension. However, there is no clear border between the linear and nonlinear deformation. To answer that, the linear model deformation should be compared with the nonlinear one. In this work, as the deformation amplitude is not a key result, for simplicity reasons, the linear material model was used.

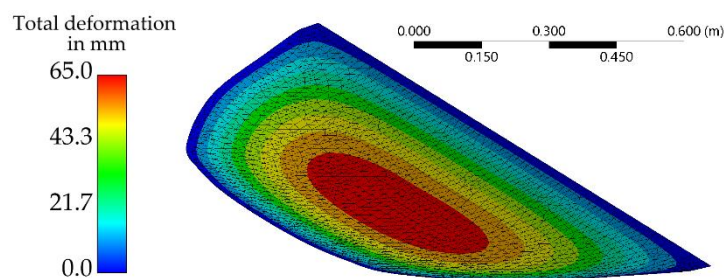


Figure 9. Magnitude of deformation of the inflatable splitter.

3.2. Passenger Car

As a preliminary analysis, the deformed splitter's shape was applied to the passenger car. In this case, the splitter deformation was calculated using an uncoupled mechanical simulation. Then, the deformed splitter geometry was added to the passengers' car geometry as a rigid body. The splitter deformation was calculated using the same numerical approach as for the Arrinera, described in the previous section.

The study analyzes the influence of a splitter in various configurations on the aerodynamic characteristics of the fastback DrivAer car. The baseline design was a vehicle without add-ons. The tested splitter was equipped with a movable flap, which allowed controlling the airflow in the channel over the splitter. Two flap setups were considered, i.e.,

open flap which allowed free flow, and a closed flap which blocked the flow and increased downforce, as shown in Figure 10.

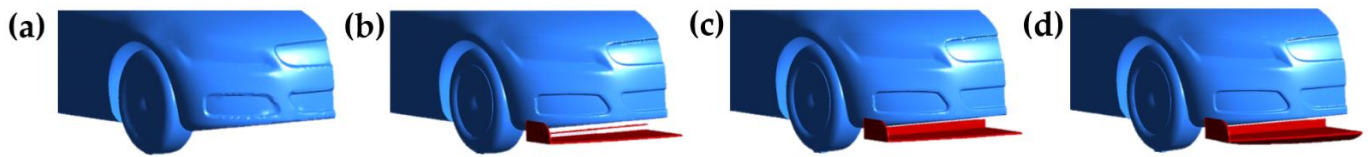


Figure 10. Analyzed variants for the DriveAer case: (a) base model without splitter; (b) open rigid splitter; (c) closed rigid splitter; (d) closed inflated splitter.

Four cases were analyzed in total. The analysis was performed at speeds of 90, 120, and 144 km/h and it was confirmed that aerodynamic force coefficients for all variants remain constant in this range of speeds.

The results of the simulations are presented in Figure 11. It can be observed that tested additional aerodynamic elements cause a moderate increase in drag compared to the base model, and a significant increase in downforce. Interestingly, even the inflated splitter, which reduced the lift coefficient by almost 0.4, did not affect the drag force value noticeably.

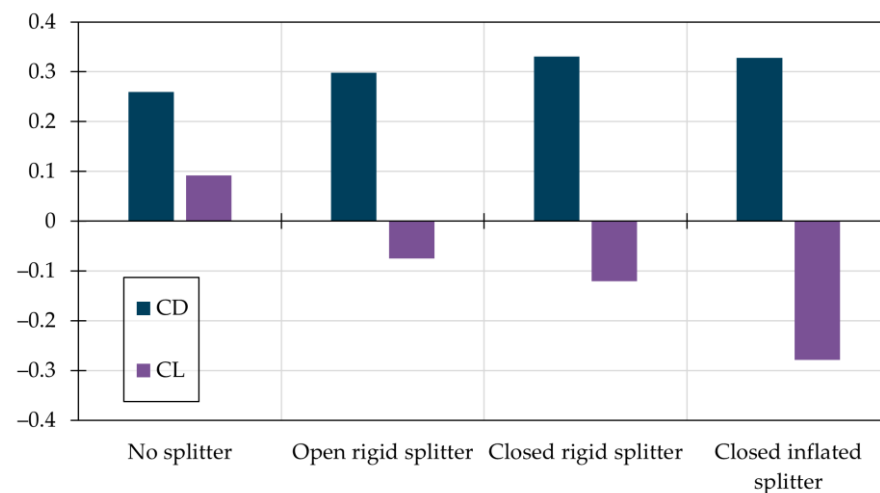


Figure 11. Drag and lift coefficients for various studied splitter variants.

The pressure coefficient contours shown in Figures 12 and 13 confirm the effectiveness of the proposed solution. No downstream elements seem to be affected by the inflated splitter.

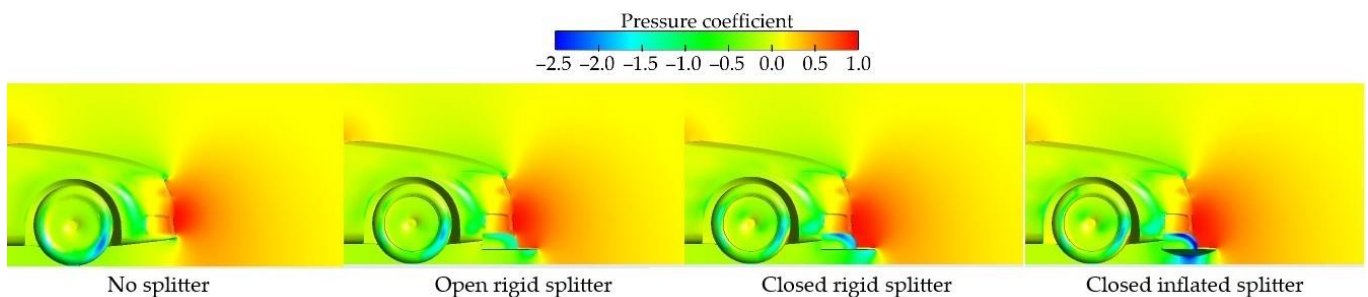


Figure 12. Pressure coefficient distribution at the symmetry plane and car body for various splitter variants.

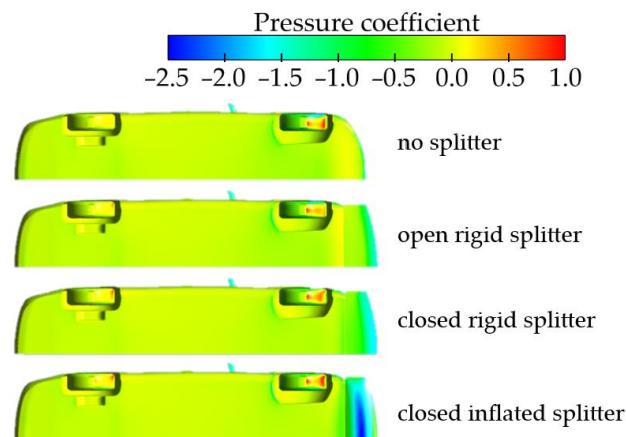


Figure 13. Pressure coefficient distribution of the car body for various splitter variants, bottom view.

The additional total downforce is applied to the front axle, as evidenced by the increased positive moment coefficient shown in Figure 14.

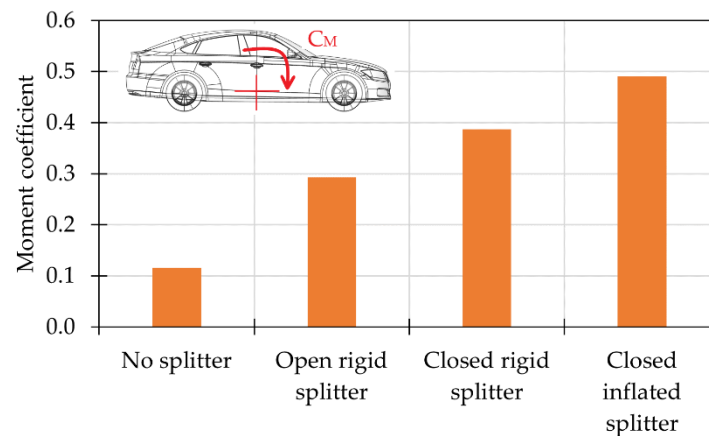


Figure 14. Moment coefficients for various studied splitter variants.

To explain how the splitter works in the configurations analyzed, the pressure distributions on the body surface in the symmetry plane are shown in Figure 15. The red color denotes the pressure differences between the upper and lower body parts generating the force that lifts these body parts upwards, the green color indicates pressing the body to the ground, and the yellow color denotes areas with zero net generated force in the vertical direction.

The effect of the splitter in all configurations is limited to a small zone in its vicinity. The splitter generates an area of pressure close to the stagnation pressure associated with the speed of the vehicle to create a downward force on the surfaces extending in front of the body. At the same time, under the rigid splitter plate near its front edge, a flow detachment area is formed with a rapidly disappearing low-pressure region which contributes to generating additional downward force on the splitter.

The splitter with a flexible bottom surface generates similarly low pressures but builds up more slowly and spreads over a larger area. Forces generated by the rigid upper surface of the splitter are similar in both versions, while the splitter with the flexible bottom surface generates a slightly higher downforce on the bottom surface with a slight increase in the aerodynamic drag force.

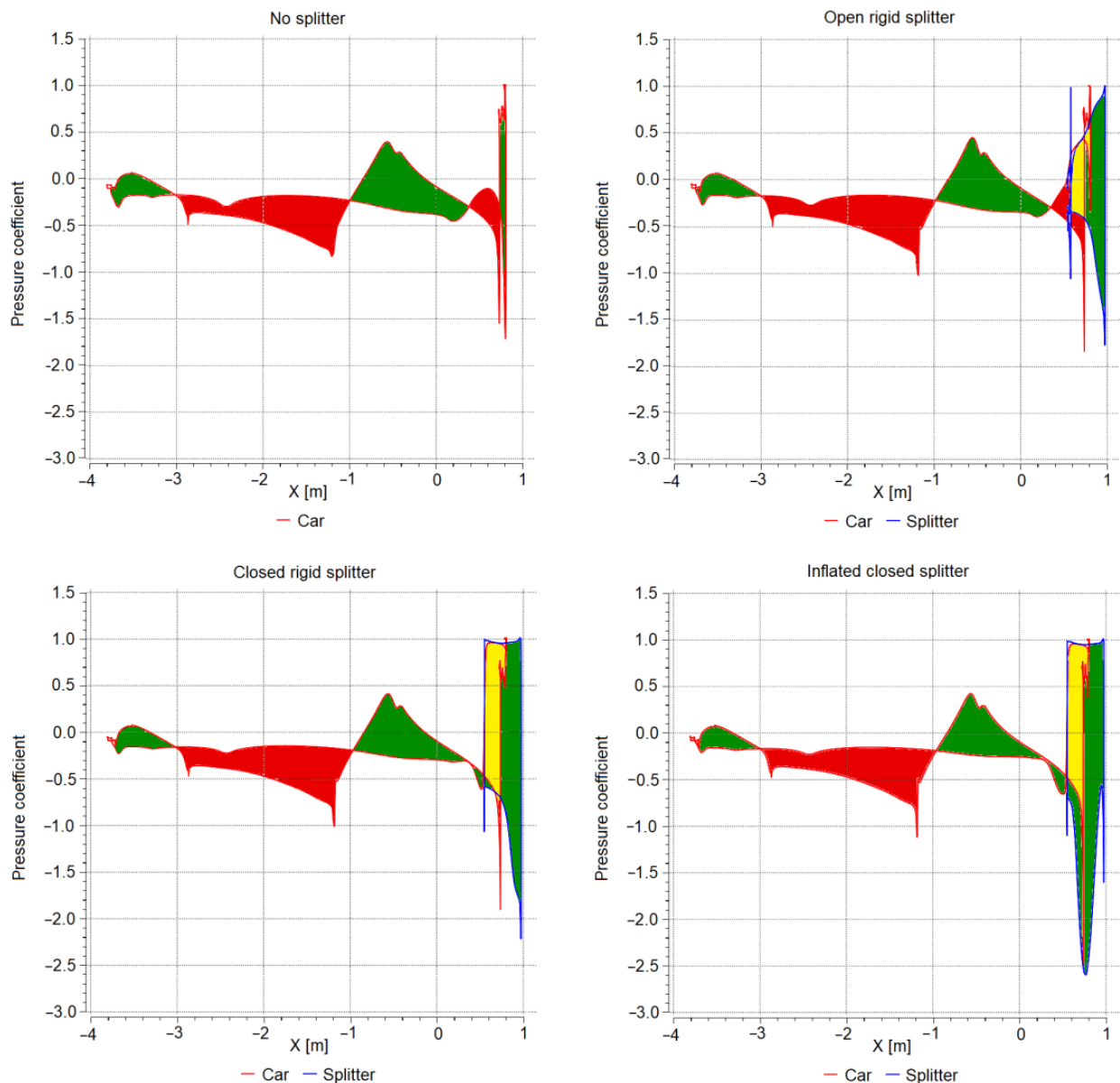


Figure 15. Pressure distribution of the symmetry plane for various studied splitter variants. Red color indicates body areas generating lift force, green colored areas generating downforce, and neutral zones are marked by yellow.

Figure 16 compares the body pressure distributions in the plane of symmetry for a car with a closed rigid splitter and a closed inflated splitter. The green color indicates areas where the inflated flexible splitter generates more downforce than the rigid splitter and the purple color indicates areas where the rigid splitter generates more downforce than the inflated splitter. The advantage of the inflatable splitter in the generation of aerodynamic downforce is clearly visible.

In the case of the previously tested models, the splitter was slightly lower than the chassis of the car. Another configuration was tested, called a high splitter, in which the splitter was attached directly to the lower surface of the bumper. Unfortunately, in this configuration adding a pumped diaphragm to the splitter did not improve the driving characteristics of the tested model, i.e., the value of the downforce practically did not change, as shown in Table 2.

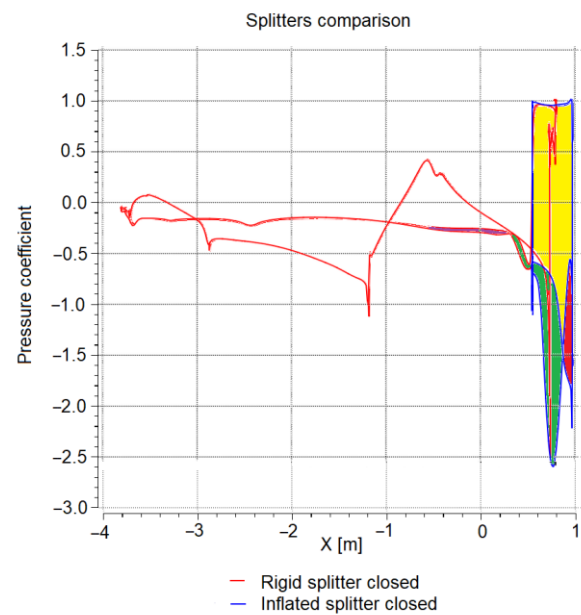


Figure 16. Pressure distribution at the symmetry plane for two studied splitter variants.

Table 2. The effect of a high splitter mount on the aerodynamic forces.

	Closed Rigid Splitter, High Mount	Closed Inflated Splitter, High Mount
Drag coefficient	0.30	0.29
Lift coefficient	0.00	−0.01

The pressure distribution for the car model with the low mount of the inflatable splitter (Figure 17) indicates a low-pressure area under the bulging splitter surface, as opposed to the high position of the inflatable splitter. In the case of a low position of the inflatable splitter, a negative pressure is created under the inflated splitter due to the acceleration of the airflow, while in the case of a high position of the splitter, the flow slows down and a positive pressure is created, which reduces the downforce effect. The velocity distribution around the car model with the inflatable splitter lowered shows a high velocity underneath and no increase in velocity at the high position of the inflatable splitter. Tested configurations with a high rigid splitter and an inflatable splitter proved to be ineffective.

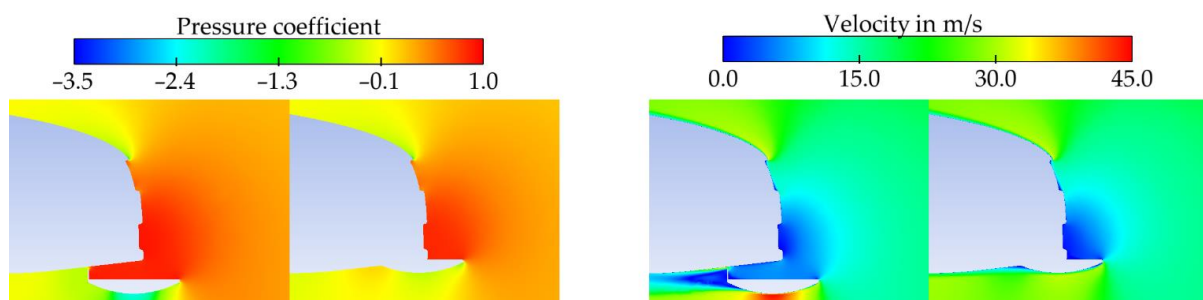


Figure 17. Pressure and velocity magnitude distribution at the symmetry plane for two studied inflated splitter positions—low mount and high mount.

It can be concluded that in the case of a passenger car characterized by a high value of underbody clearance, the prerequisite for proper operation of the splitter with the inflated diaphragm is a small distance between the roadway and the lowest surface of the splitter. This opens a wide area for the use of inflatable splitters with a shape controlled only by the

pressure inside of them. In the case of a passenger car, the car directional characteristics can be changed smoothly towards oversteer by adjusting the pressure inside the splitter.

3.3. Sports Car

3.3.1. Zero Pitch Angle

As a continuation of the work carried out on passenger cars, the deformed splitter was mounted on the sports car Arrinera Hussarya. In such cars, it is important to provide a proper force balance between the front and rear axles to maximize performance on the track. The reference Arrinera Hussarya model had no splitter and it was equipped with a rear spoiler. Different configurations were tested, which are shown in Figure 18.

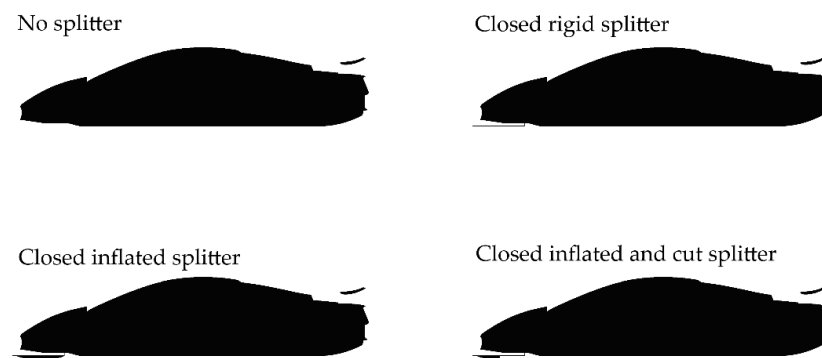


Figure 18. Studied splitter variants for the Arrinera Hussarya case.

The cut splitter shown in Figure 18 is based on the inflated splitter. It was cut in half, expecting that the sharp edge would induce flow separation. Thus, it would lead to a pressure decrease under the front axle and a downforce increase.

The pressure coefficient distribution on the symmetry plane for all configurations is presented in Figure 19. It can be seen that using any type of splitter decreases the pressure coefficient around the car front, leading to a downforce increase in that region. Obviously, the biggest effect of the splitter is in the front part of the car but it also influences the flow in the rear axle region negatively. This effect is better observable in Figure 20 where streamlines are presented.

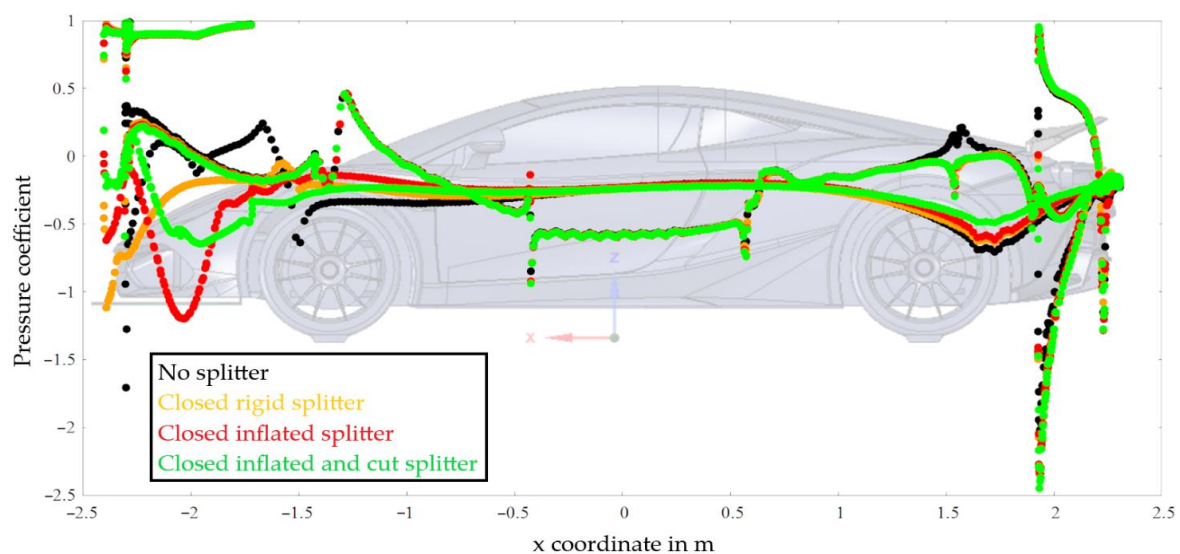


Figure 19. Pressure coefficient distribution on the symmetry plane along the car body for the baseline case and various studied splitter variants.

Drag and lift coefficients are presented in Figure 21. In the case of Arrinera Hussarya, the projected frontal area was 2.1 m^2 . Total downforce did not change significantly if the elastic splitter was used instead of a rigid one. However, the distribution of this force is shifted towards the front axle, as shown in Figure 22. The total downforce does not increase as the splitter with low ground clearance disrupts the operation of the diffuser.

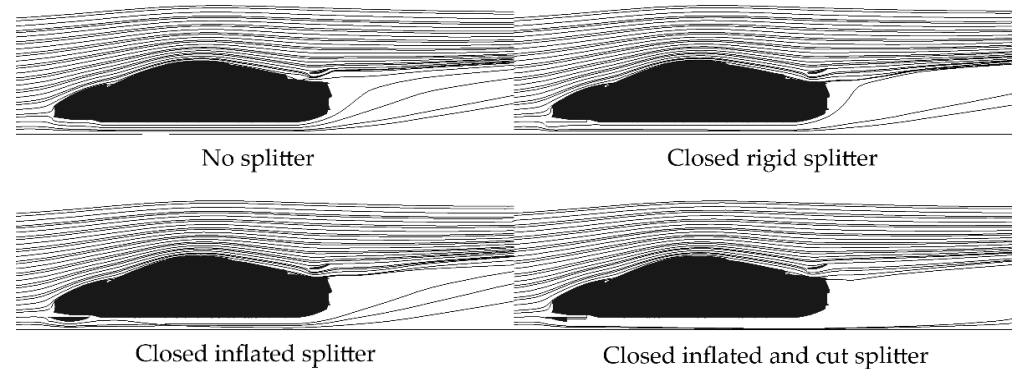


Figure 20. Pathlines released from a line in the symmetry plane for the baseline case and various studied splitter variants.

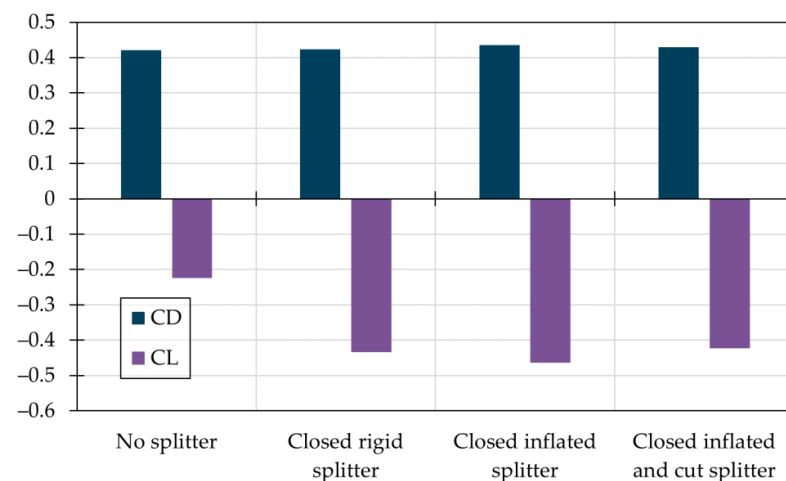


Figure 21. Drag and lift coefficients for various splitter configurations.

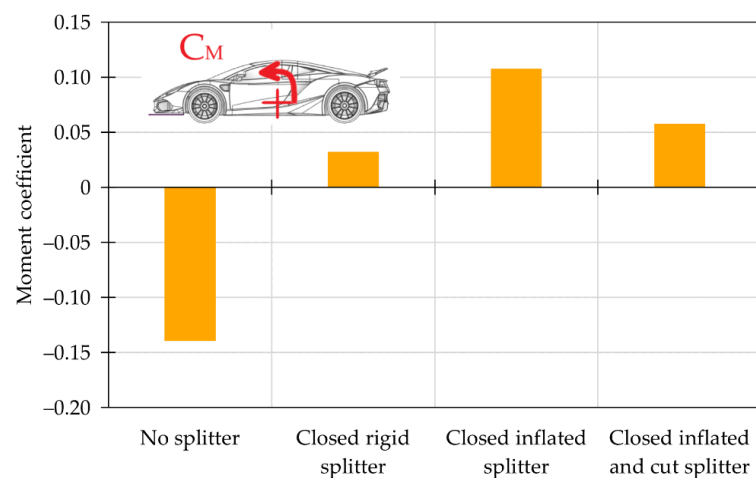


Figure 22. Moment coefficient for various splitter configurations.

Surprisingly, a slightly lower value of downforce was observed for the cut splitter configuration than for the uncut.

The moment coefficients are shown in Figure 22. It can be seen that the baseline configuration without splitter results in a negative moment. The largest positive moment is obtained for the closed inflated splitter variant. The summary of all coefficients is also presented in Table 3.

Table 3. Drag, lift, and moment coefficients for various splitter configurations.

Splitter Variant	C_D	C_L	C_M
No splitter	0.421	−0.224	−0.139
Closed rigid splitter	0.424	−0.434	0.032
Closed inflated splitter	0.435	−0.464	0.108
Closed inflated and cut splitter	0.429	−0.423	0.058

The contours of the pressure coefficient and velocity magnitude are presented in Figures 23–25. An enlarged low-pressure zone is observed for the inflated splitter. Interaction between the splitter and the diffuser is also visible. The cut splitter design, although it induced separation and provided a larger area of the low-pressure zone, did not manage to provide adequately low pressure values. In total, the uncut inflated design remained superior.

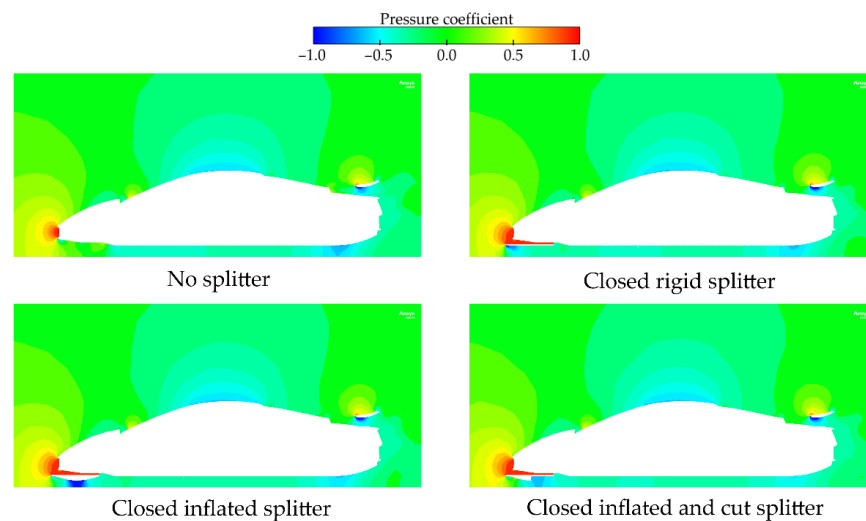


Figure 23. Pressure contours on the symmetry plane for various splitter configurations.

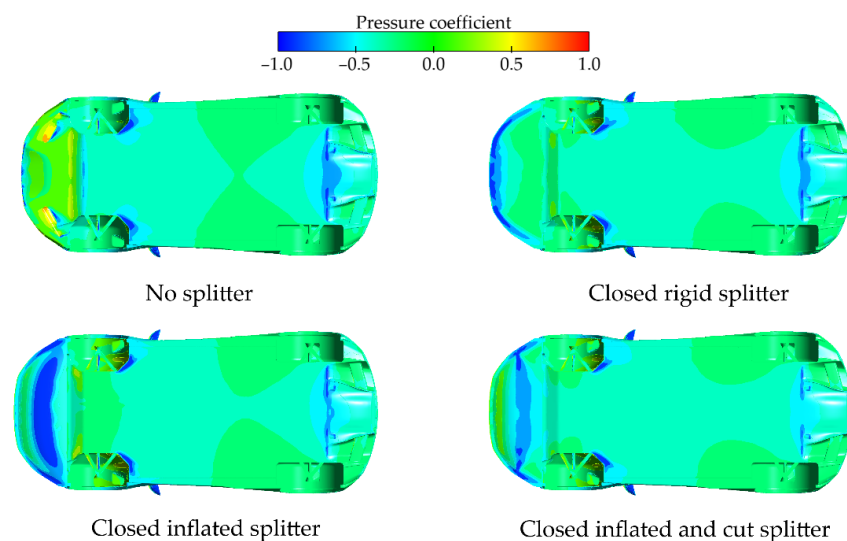


Figure 24. Pressure coefficient contour for various splitter configurations, bottom view.

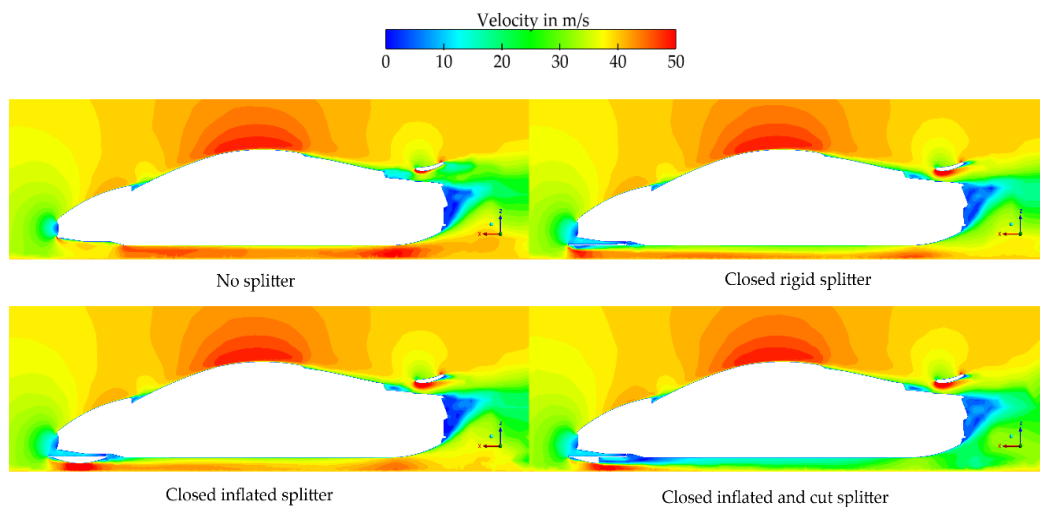


Figure 25. Velocity magnitude contours on the symmetry plane for various splitter configurations.

3.3.2. Nonzero Pitch Angle

When driving on a hilly track, conditions that promote front end lift occur at the top of the track. In addition, driving close to the aerodynamic wake generated by the preceding vehicle can reduce the front axle downforce [7].

For this reason, another analysis, using the Arrinera Hussarya model as an example, examined the effect of a flexible splitter on forces and moments with increasing pitch angle.

The model for this study is shown in Figure 26a. Simulations were performed for three pitch angles: 0, 1, and 2 degrees. The car was pitched with respect to an axis, which was 0.45 m from the ground, at a distance of $\frac{3}{4}L$ from the front axle, where L is the distance between axles.

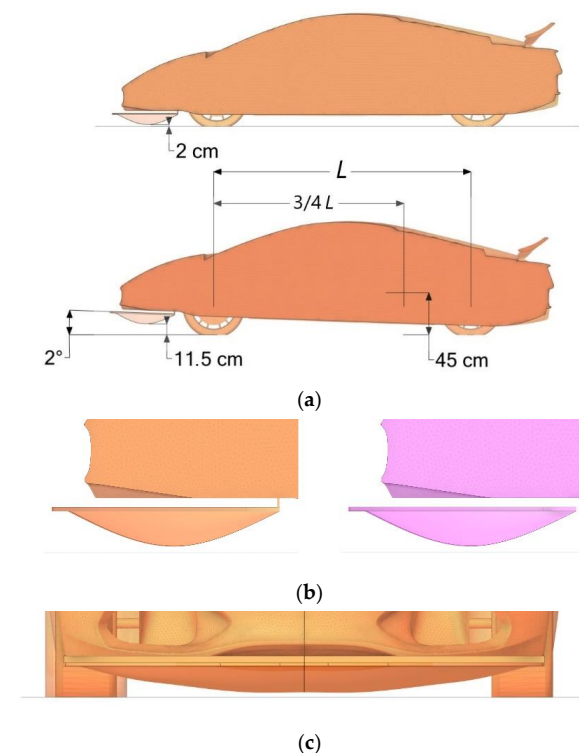


Figure 26. Geometry used for the pitching moment study: (a) car outline view (symmetric half of the model); (b) elastic splitter with a closed and opened gap, side view; (c) elastic splitter, front view.

From the previous analyses, it was determined that low ground clearance is required for the splitter to work properly. The following models were made: without a splitter, with a flat splitter, and with a flexible splitter, which was deformed enough to have a ground clearance of 2 cm. The deformed splitter was also tested in both closed and opened variants, as shown in Figure 26b. The front view of the inflated splitter with lower ground clearance is shown in Figure 26c. The analyses were performed for a different model of the Arrinera Hussarya vehicle than in the previous section, with lower overall ground clearance. Hence, slightly different results will be observed for the no-splitter variant.

Obtained results are summarized in Table 4. Moment coefficients were determined with the use of a reference area of 1.0382 m², which corresponds to a symmetric half of the model. The reference area was kept constant regardless of the pitching angle. C_{Lf} and C_{Lr} are lift coefficients at the front and rear axle, correspondingly. Additionally,

$$C_L = C_{Lf} + C_{Lr}. \quad (1)$$

Table 4. Influence of flexible splitter on aerodynamic forces and moment coefficients for various pitch angles.

Splitter	Pitch Angle in Degrees	C_D	C_L	C_{Lf}	C_{Lr}	C_M
None	0	0.449	−0.212	0.049	−0.261	−0.143
Rigid closed	0	0.477	−0.441	−0.298	−0.143	0.071
Inflated open	0	0.474	−0.490	−0.421	−0.069	0.163
Inflated closed	0	0.495	−0.284	−0.385	0.101	0.225
None	1	0.507	−0.013	0.189	−0.202	−0.180
Rigid closed	1	0.513	−0.248	−0.072	−0.176	−0.048
Inflated open	1	0.506	−0.338	−0.178	−0.160	−0.008
Inflated closed	1	0.515	−0.443	−0.308	−0.135	0.080
None	2	0.532	0.124	0.323	−0.199	−0.241
Rigid closed	2	0.547	−0.018	0.108	−0.126	−0.107
Inflated open	2	0.530	−0.041	0.071	−0.112	−0.084
Inflated closed	2	0.548	−0.230	−0.053	−0.177	−0.057

In Figure 27, a data snippet concerning the drag coefficient is presented. Introducing a deformed splitter with a closed gap at zero pitching angle increases the drag by 10% in comparison to the geometry without a splitter. This is because of the low clearance between splitter and ground, which introduces a significant stagnation zone at the vehicle front. At higher pitching angles, clearance increases and all of the models had a similar drag coefficient with a 5% difference between variants. The effect can be observed on velocity and pressure contours of the symmetry plane, shown in Figures 28 and 29.

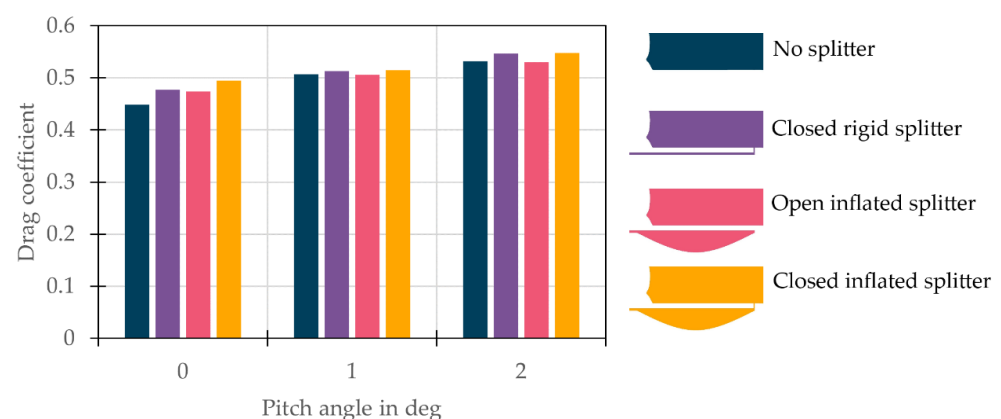


Figure 27. Influence of different splitter configurations on drag coefficient; various pitch angles.

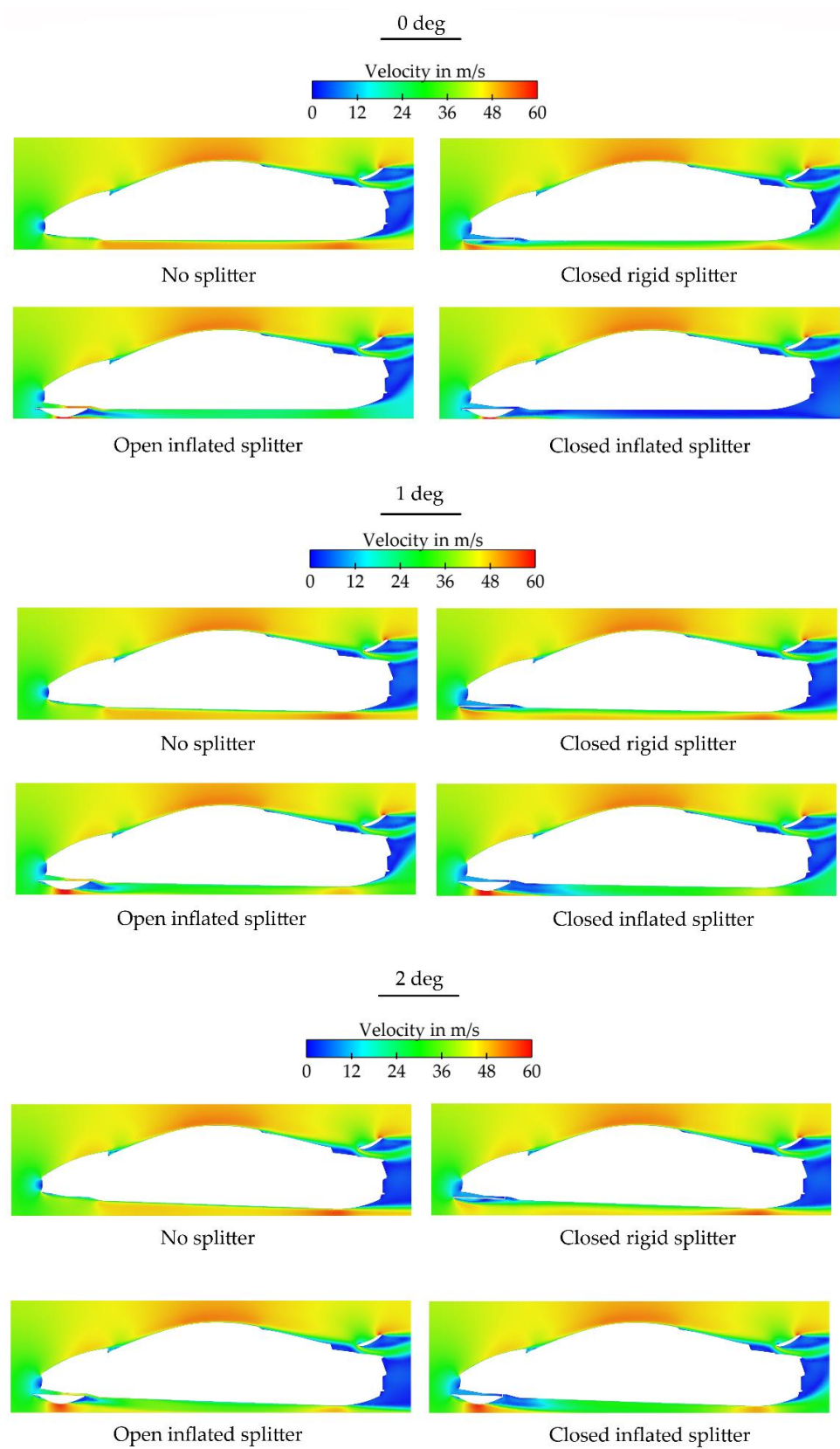


Figure 28. Velocity magnitude contours of the symmetry plane for various splitter configurations and pitching angles.

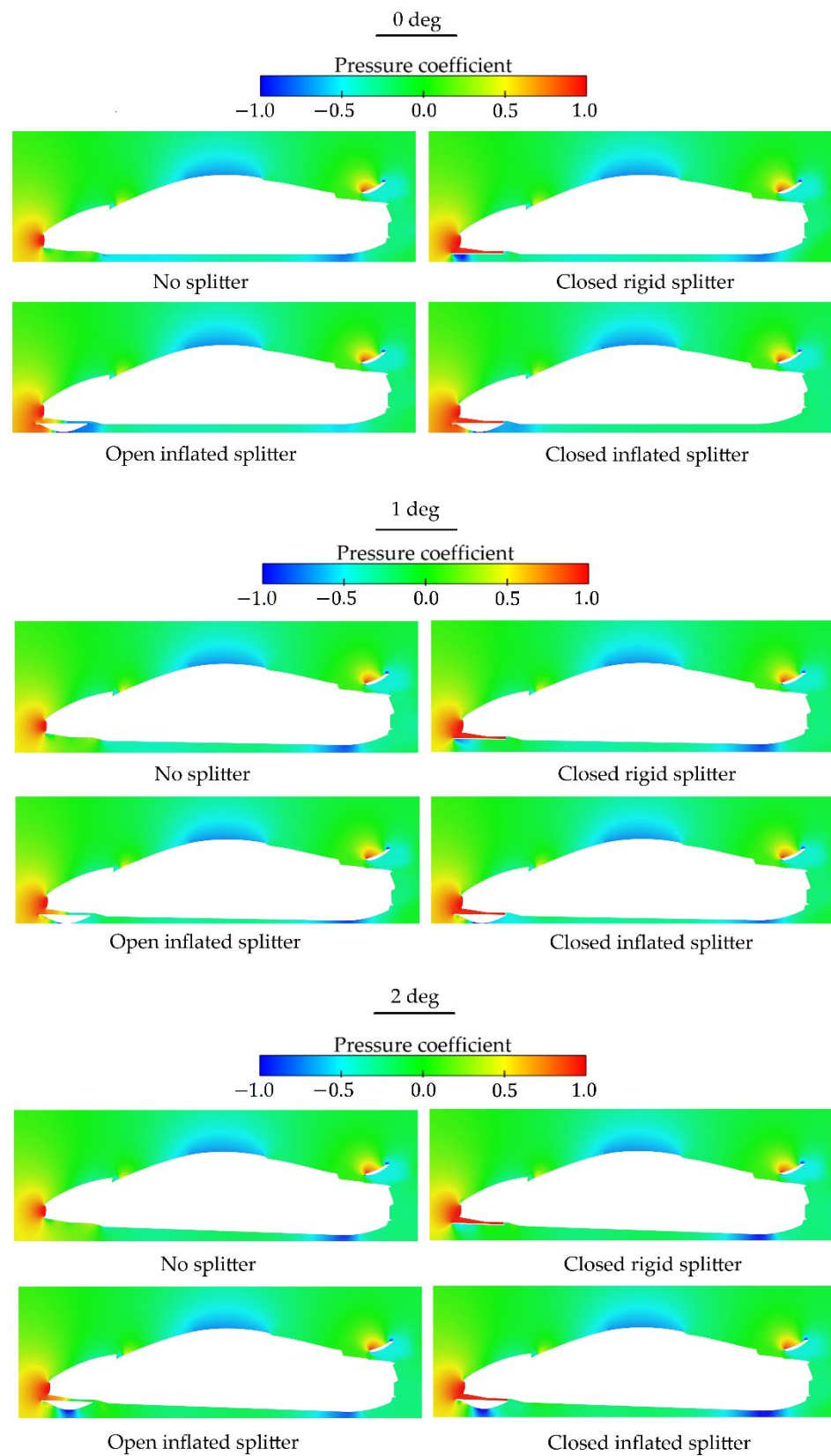


Figure 29. Pressure coefficient of the symmetry plane for various splitter configurations and pitching angles.

Looking at the lift coefficient in Figure 29, one can observe a significant aerodynamic downforce introduced by the splitter.

For zero pitching angle, the variant with an opened gap performs better than the closed one. This is due to flow blockage in the variant with a closed gap, which affects all the downstream elements of vehicle aerodynamics. Most importantly, it eliminates the action of the diffuser. One can confirm in Figure 30 that in both flexible splitter variants for the zero pitching angle, the front lift coefficient remains similar, while the rear lift coefficient is unfavorable for the variant with the closed gap. This is also seen in the pressure coefficient of the bottom surface, presented in Figures 31 and 32. For larger pitching angles, the clearance increases and the diffuser operates for the closed-gap splitter variant even better than for the baseline case with a flat splitter.

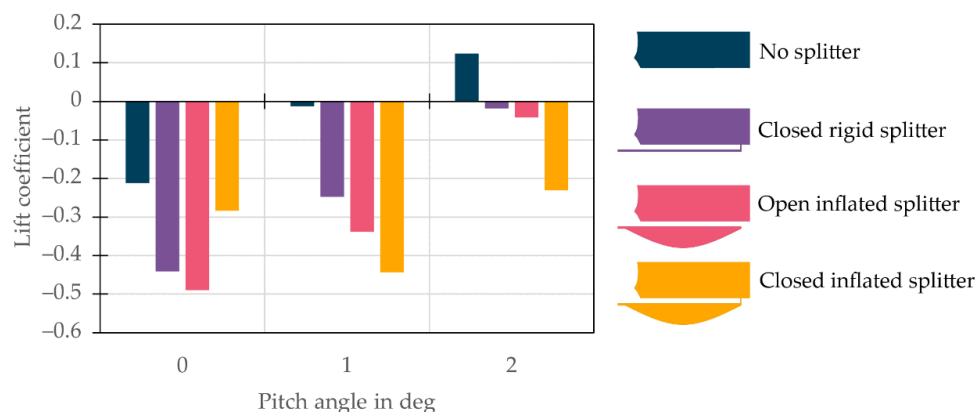


Figure 30. Influence of different splitter configurations on lift coefficient; various pitch angles.

This result seems positive. Total downforce is increased in comparison to the baseline variant with a flat splitter, even when a positive pitching angle is introduced.

However, from the point of view of vehicle longitudinal stability, the distribution of this increased downforce is crucial.

As shown in Figure 33, for zero pitching angle, the inflated splitter introduces significant downforce on the front axle. The rear axle is lifted due to an inactive diffuser. The splitter solution remains valid up to the pitching angle of ca. 1.5 degrees. For 2-degree pitch, forces acting on the rear axle outweigh the front axle forces.

Without the splitter, forces acting on the rear axle clearly dominate from the zero pitching angle. This disproportion increases with increasing pitch.

The flap opening or closing the channel over the rigid splitter wall can be used to choose the proper configuration depending on the pitching angle: opened at zero pitch angle, closed at higher pitch angles.

In the case of a sports car with low ground clearance and additional aerodynamic elements at the rear of the body (diffuser), the situation is different than in the case of passenger cars with high ground clearance. For a car pitch angle of 0 and very low ground clearance under the inflatable splitter and a closed channel above the splitter, not enough air flows under it for the rear diffuser to work effectively. This configuration is advantageous when it is intended to prevent front underflow. Opening the flow in the channel above the inflatable splitter allows enough air to supply the rear diffuser to operate. With a larger pitch angle, the gap under the inflatable splitter is large enough to ensure the rear diffuser works.

This case study can be summarized with Figure 34, which presents the pitching moment coefficient. The positive moment coefficient indicates dominating downforce on the front axle. Without any splitter, a negative pitching moment is observed for all studied pitch angles. For the case with a flat splitter, the moment coefficient starts low at zero pitch angle and becomes negative at approx. 0.5-degree pitch angle. Introducing a flexible splitter with a closed gap provides an effective solution to prevent further vehicle pitching up to an angle of 1.5 degrees.

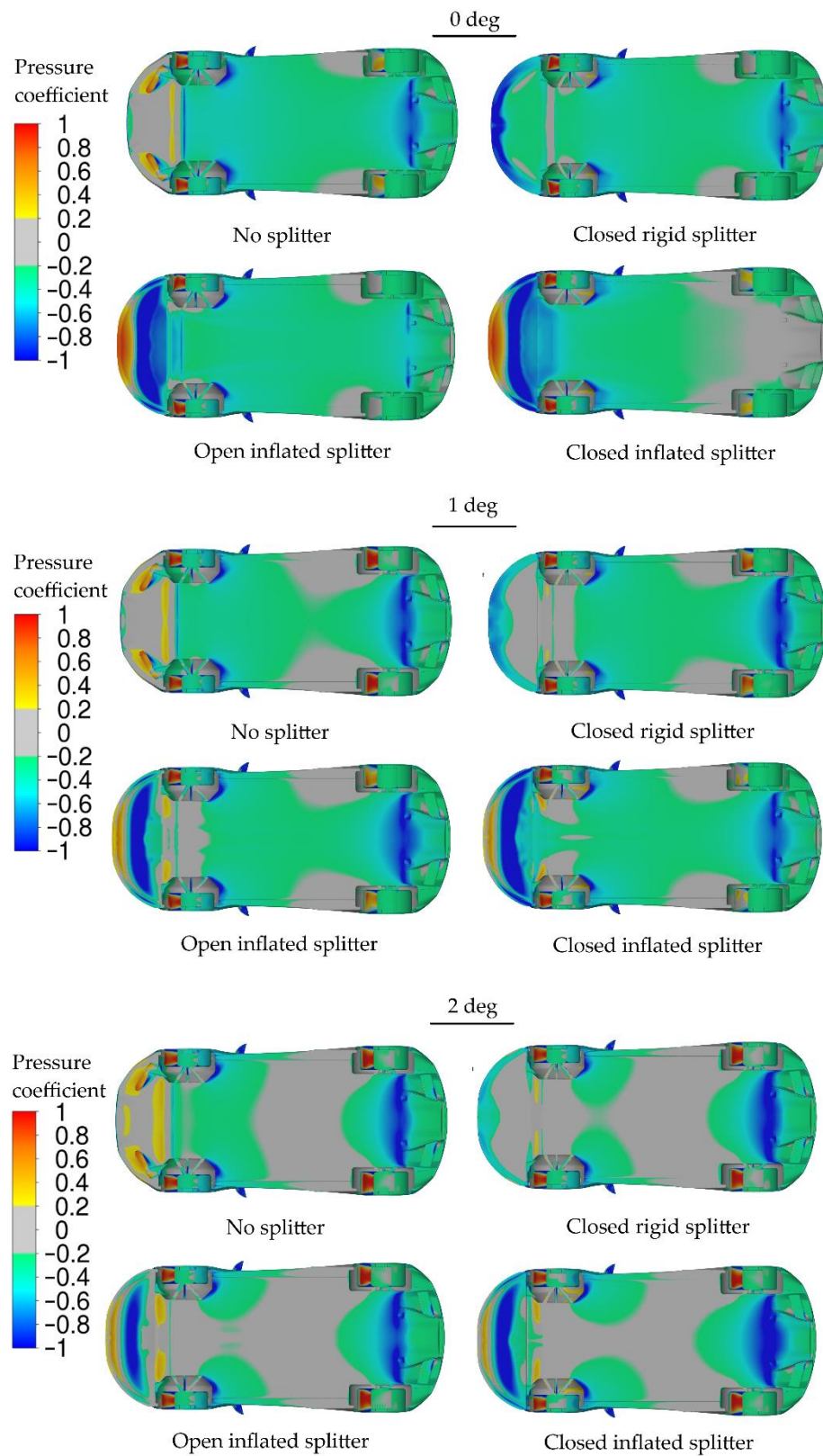


Figure 31. Pressure coefficient for various splitter configurations and pitching angles, bottom view.

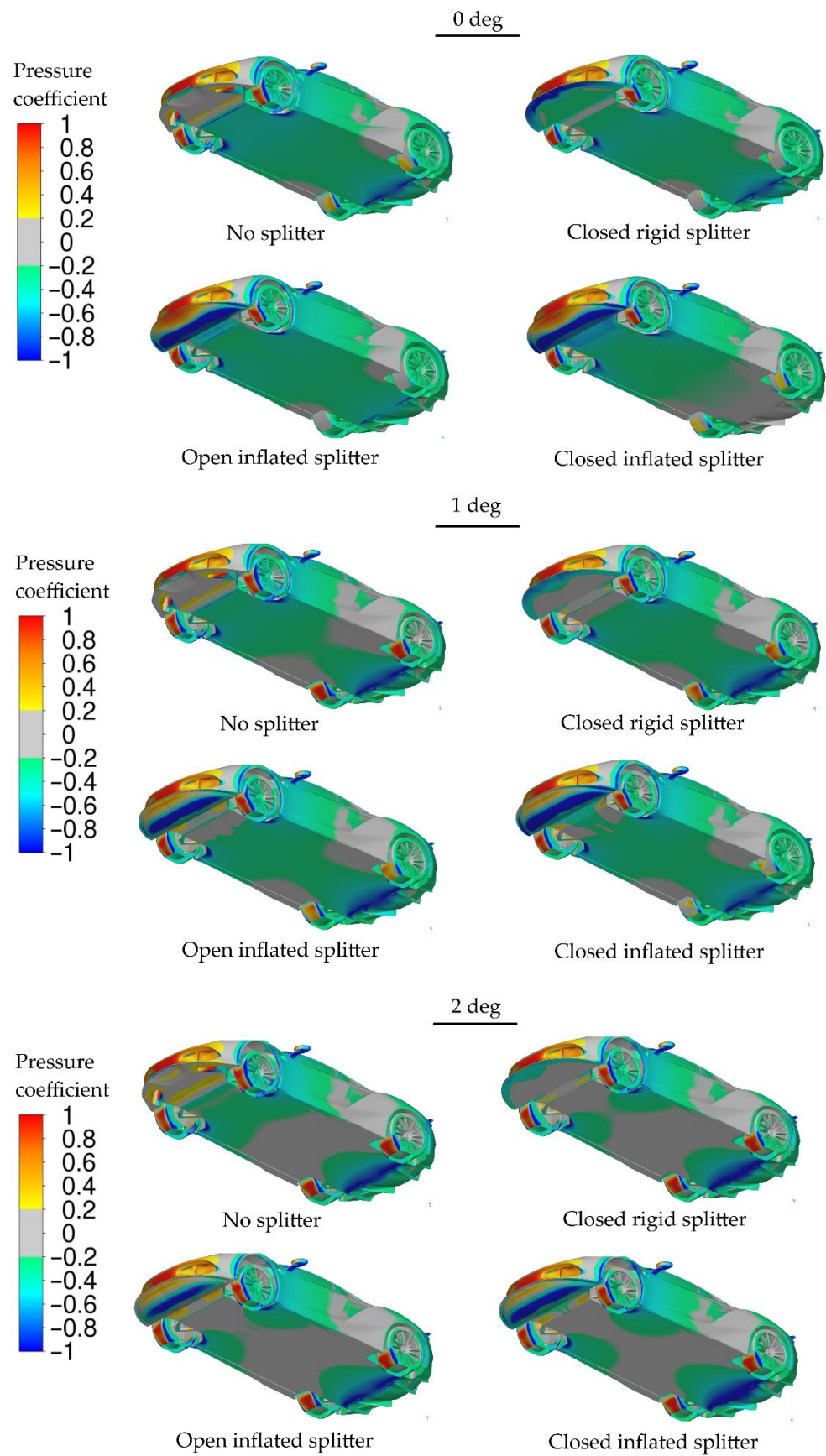


Figure 32. Pressure coefficient for various splitter configurations and pitching angles, bottom angled view.

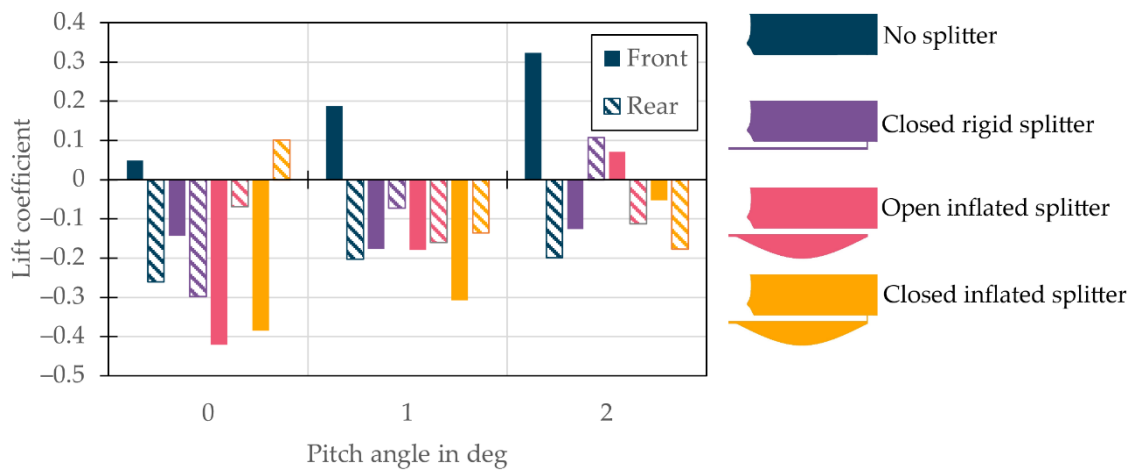


Figure 33. Influence of different splitter configurations on front and rear axle lift coefficients; various pitch angles.

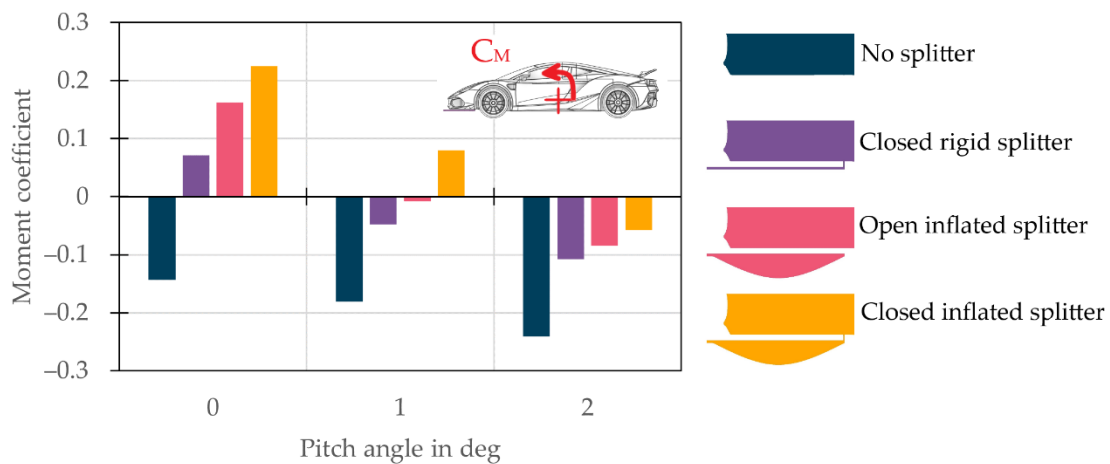


Figure 34. Influence of different splitter configurations on pitching moment coefficient; various pitch angles.

The analyses presented here were an attempt to address the problem of vehicle pitching stability. Static cases were studied, for stationary geometry. As the effectiveness of the proposed solution was confirmed, transient analyses can be performed in future, where vehicle motion will be resultant.

4. Conclusions

In the age of electric cars, one must consider the energy consumption of various devices, such as air conditioning, battery cooling, lights, braking and steering systems, etc. The proposed solution of an elastic splitter provides additional downforce, which allows safe driving through corners at high speed. Reducing the travel time will reduce the time of using all the additional components, and indirectly translates to energy savings.

In the case of passenger cars, the proposed solution was effective in providing significant downforce for the front axle and the total downforce increased with a slight increase in the drag force. The requirement for good performance of the splitter is low ground clearance. By adjusting the pressure inside the splitter, the car's directional characteristics can be changed smoothly towards oversteer characteristics.

In the case of a sports car, an inflatable elastic splitter did not increase the total downforce, due to the interaction of the splitter with the diffuser. However, downforce distribution shifted towards the front axle. The solution was also effective in the case of a nonzero pitch angle. In this scenario, the flexible splitter provided not only a pitching

moment towards the front axle, but also increased overall downforce. Splitter performance can be controlled by the pressure between deforming and rigid plates, as well as by the flap which opens or closes the channel over the rigid splitter wall. For a sports car in races with not-so-rigid regulations, such as Time Attack races, a more inflated splitter can provide effective front axle downforce during acceleration and after depressurization during braking.

For other classes of racing, it could provide an emergency system to save the vehicle if the front end of the car is lifted, by explosive inflation of the space above the flexible shell. Which, while excluding the vehicle from classification for that race, would protect the vehicle from strong damage.

A movable flap closing the tunnel between the body and the splitter, due to its low inertia, can be used as an element generating, together with the splitter, rapid changes in the vertical force acting in this flow area on the car body. Proper control systems can be used for damping high-frequency (10 Hz) vertical car body oscillations.

In this paper, only stationary solutions were presented in order to evaluate if this type of solution has potential advantages. Further work is planned to develop a transient flow model including both body motion and transient filling processes in the space between the elastic surface of the splitter and its rigid part.

Author Contributions: Conceptualization, J.P.; methodology, M.S., K.K., S.T. and J.P.; software, M.S., K.K. and S.T.; validation, M.S., K.K., S.T. and J.P.; formal analysis, M.S., K.K., S.T. and J.P.; investigation, M.S., K.K., S.T. and J.P.; resources, M.S., K.K., S.T. and J.P.; data curation, M.S., K.K., S.T. and J.P.; writing—original draft preparation, J.P.; writing—review and editing, M.S., K.K., S.T. and J.P.; visualization, M.S., K.K., S.T. and J.P.; supervision, J.P. All authors have read and agreed to the published version of the manuscript.

Funding: This research received no external funding.

Data Availability Statement: Not applicable.

Acknowledgments: The authors thank Arrinera SA for allowing the geometry of the Hussarya vehicle to be used to perform the aerodynamic analyses presented in this paper.

Conflicts of Interest: The authors declare no conflict of interest.

Appendix A

Dominy et al.'s paper [14] presents the results of analysis of the accident at the Le Mans track in 1999 and the results of experimental tests in the wind tunnel of the model equivalent of the Mercedes CLR car involved in the accident, for a range of pitch angles. The authors of [14] presented the results of the measurements in the form of changes in aerodynamic forces for a speed of 320 km/h, explaining that this form of results is more readable for potential users.

For comparison purposes, for the analyzed prototype of the Hussarya sports car with an assumed maximum speed of 360 km/h, the values of the components of the downforce for 320 km/h were calculated.

Figure A1 shows a comparison of the total, rear, and front axle downforce between the Hussarya with a rigid flat splitter and LMP car [14]. Although the two car models represent high-speed cars with different purposes, significant similarities in their aerodynamic characteristics can be noted. It should also be noted here that, in general, cars of this era (1999) generated low downforce, especially in the Le Mans configuration. The total downforce is similar, that of the Hussarya car is slightly smaller, and with the increase in the pitch angle they change in a similar manner. The downforce of the front axle of the Hussarya is slightly higher and that of the rear axle slightly lower. The nature of their changes with a change in pitch angle is identical.

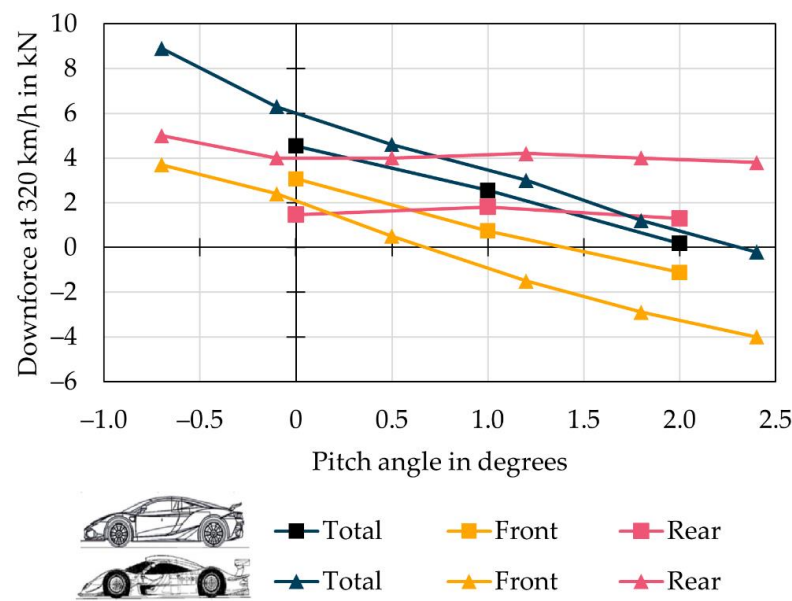


Figure A1. Comparison of changes in aerodynamic downforce and its distribution to the front and rear axles as a function of body tilt angle, calculated for a Hussarya car with a flat rigid splitter and a closed channel above it, against experimental results of a model of an LMP-class car presented in [14].

Subsequent figures will illustrate the influence of the inflatable splitter on the Hussarya car in the context of comparison with the LMP-class car. Using an inflatable splitter with an open channel above it raised the level of aerodynamic downforce to the level presented in [14]. The splitter with a closed channel above it, for a body tilt angle of 0, generates a significantly lower total downforce. With an increase in the body tilt angle, the downforce increases, exceeding the values generated by the inflated splitter with an open channel.

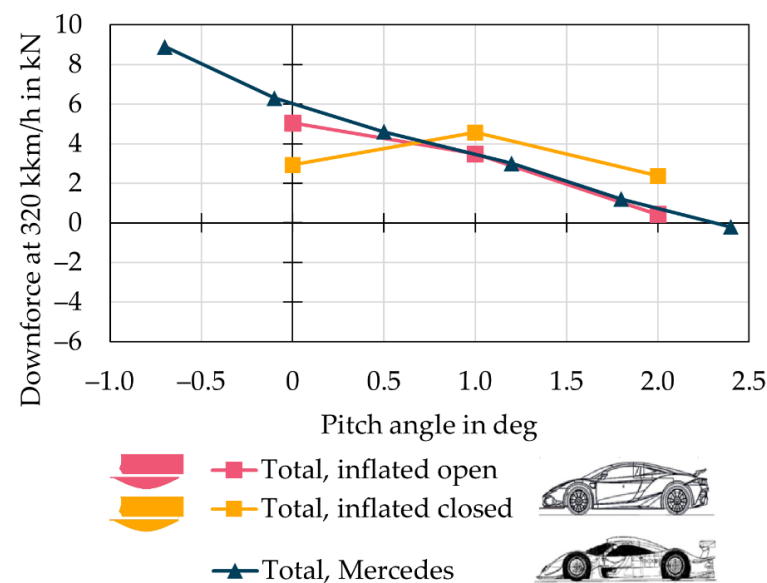


Figure A2. Changes in the total aerodynamic downforce of a Hussarya car equipped with an inflatable splitter with an open channel above it and a closed channel, against experimental results of a model of an LMP-class car presented in [14].

Figure A3 shows the component of downforce acting on the front axle. An inflatable splitter with a closed channel above it, for a body tilt angle of 0, generates almost identical downforce on the front axle. With an increase in the angle of body tilt, the downforce

increases, significantly exceeding the values generated by the inflatable splitter with an open channel.

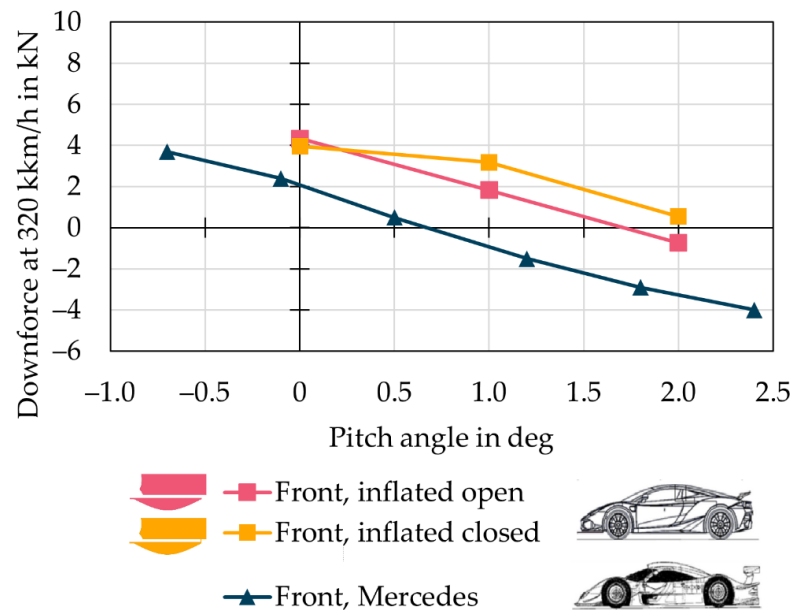


Figure A3. Changes in the aerodynamic downforce acting on the rear axle of a Hussarya car equipped with an inflatable splitter with an open channel above it and a closed channel, against the results of measurements of the car model in [14].

As can be seen by comparing the data in Figure A4, using an inflatable splitter with an open channel above it, the level of aerodynamic downforce was slightly reduced below that generated by a rigid splitter with a closed channel. An inflatable splitter with a closed channel above it, for a body tilt angle of 0, generates significantly lower downforce on the rear axle. With an increase in the body tilt angle, the downforce increases to the values generated by the inflatable splitter with an open channel. The downforce on the rear axle of the Hussarya car with an inflatable splitter is similar to that obtained with a rigid splitter.

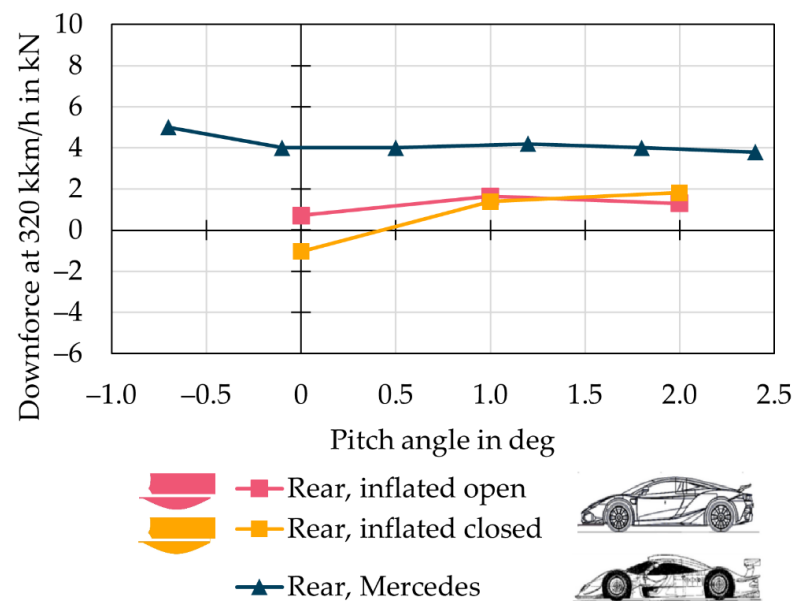


Figure A4. Changes in the aerodynamic downforce acting on the rear axle of a Hussarya car equipped with an inflatable splitter with an open channel above it and a closed channel, against the background of the results of measurements of the car model in [14].

The effect of opening or closing the channel over the inflatable splitter can be explained as follows: for a body pitch angle of 0, the outer surface of the splitter is very close to the ground, blocking air flow to the diffuser at the body rear when the channel over the splitter is closed. The rear axle downforce decreases. Opening the duct increases the airflow through the diffuser resulting in an increase in rear axle downforce. When the body angle increases, the clearance under the inflatable splitter increases and the airflow through the diffuser increases and the effect of opening the channel over the splitter disappears.

References

1. Milliken, W.F.; Milliken, D.L. *Race Car Vehicle Dynamics*; SAE International: Warrendale, PA, USA, 1995.
2. Katz, J. *Race Car Aerodynamics: Designing for Speed*, 2nd ed.; Bentley (Robert) Inc.: Cambridge, MA, USA, 1996.
3. Katz, J. Aerodynamics in motorsports. *Proc. Inst. Mech. Eng. Part P J. Sports Eng. Technol.* **2019**, *235*, 1–15. [[CrossRef](#)]
4. Dominy, R.G. Aerodynamics of Grand Prix Cars. *Proc. Inst. Mech. Eng. Part D J. Automob. Eng.* **1992**, *206*, 267–274. [[CrossRef](#)]
5. Porcar, L.; Toet, W.; Gamez-Montero, P.J. Study of the Effect of Vertical Airfoil Endplates on Diffusers in Vehicle Aerodynamics. *Designs* **2021**, *5*, 45. [[CrossRef](#)]
6. Huminic, A.; Huminic, G. Aerodynamics of curved underbody diffusers using CFD. *J. Wind Eng. Ind. Aerodyn.* **2020**, *205*, 104300. [[CrossRef](#)]
7. Guerrero, A.; Castilla, R.; Eid, G. A Numerical Aerodynamic Analysis on the Effect of Rear Underbody Diffusers on Road Cars. *Appl. Sci.* **2022**, *12*, 3763. [[CrossRef](#)]
8. Ehirim, O.H.; Knowles, K.; Saddington, A.J. A review of ground-effect diffuser aerodynamics. *J. Fluids Eng.* **2019**, *141*, 1–19. [[CrossRef](#)]
9. Zhang, X.; Toet, W.; Zerihan, J. Ground effect aerodynamics of race cars. *Appl. Mech. Rev.* **2006**, *59*, 33–49. [[CrossRef](#)]
10. McBeath, S. *Competition Car Aerodynamics*, 3rd ed.; Veloce Publishing: Dorchester/Poundbury, UK, 2017.
11. Piechna, J. A Review of Active Aerodynamic Systems for Road Vehicles. *Energies* **2021**, *14*, 7887. [[CrossRef](#)]
12. Szudarek, M.; Piechna, J. CFD Analysis of the Influence of the Front Wing Setup on a Time Attack Sports Car's Aerodynamics. *Energies* **2021**, *14*, 7907. [[CrossRef](#)]
13. Wright, P. Cleared for take-off. *Racecar Eng.* **1999**, *9*, 16–18.
14. Dominy, R.G.; Ryan, A.; Sims-Williams, D.B. The aerodynamic stability of a Le Mans prototype race car under off-design pitch conditions. *SAE Trans.* **2000**, *109*, 1454–1460.
15. Katz, J.; Garcia, D.; Sluder, R. *Aerodynamics of Race Car Liftoff*; SAE Technical Paper Series; SAE International: Warrendale, PA, USA, 2004. [[CrossRef](#)]
16. Porsche GT1 Yannick Dalmas Road Atlanta Crash. Available online: <https://www.youtube.com/watch?v=NTSdaILo4L4> (accessed on 31 June 2022).
17. Gullberg, P.; Löfdahl, L. *The Role of Aerodynamics in the 1955 Le Mans Crash*; SAE Technical Paper 2008-01-2996; SAE International: Warrendale, PA, USA, 2008. [[CrossRef](#)]
18. Kataoka, T.; China, H.; Nakagawa, K.; Yanagimoto, K.; Yoshida, M. Numerical simulation of road vehicle aerodynamics and effect of aerodynamic devices. *SAE Trans.* **1991**, *100*, 722–734.
19. Santer, R.; Gleason, M.E. *The Aerodynamic Development of the Probe IV Advanced Concept Vehicle*; SAE Technical Paper Series; SAE International: Warrendale, PA, USA, 1983; p. 831000. [[CrossRef](#)]
20. Estrada, G. Mercedes-AMG GTR: Aerodynamics for the Record. In Proceedings of the Progress in Vehicle Aerodynamics and Thermal Management, 11th FKFS Conference, Stuttgart, Germany, 26–27 September 2017; pp. 135–144. [[CrossRef](#)]
21. Meder, J.; Wiegand, T.; Pfadenhauer, M. Adaptive aerodynamics of the new Porsche 911 Turbo. *ATZ Worldw.* **2014**, *116*, 42–45. [[CrossRef](#)]
22. Bhattacharjee, S.; Arora, B.; Kashyap, V. *Optimization of Race Car Front Splitter Placement Using CFD*; SAE Technical Paper 2019-01-5097; SAE International: Warrendale, PA, USA, 2019. [[CrossRef](#)]
23. Cupis, D.D.; Carvalho Pinheiro, H.D.; Ferraris, A.; Airale, A.G.; Carello, M. Active Aerodynamics Design Methodology for Vehicle Dynamics Enhancement. In Proceedings of the International Conference of IFToMM ITALY, Naples, Italy, 9–11 September 2020; Springer: Cham, Switzerland, 2020; pp. 777–785.
24. Yasui, T.; Murata, O. The Effect of a Moving Ground and Rotating Wheels on Transient Aerodynamic Properties of a Car Model in Pitching Motion. *Trans. Soc. Automot. Eng. Jpn.* **2021**, *52*, 808–813.
25. Braking Bag a Braking Parachute for the Car. Available online: <https://500sec.com/braking-bag/> (accessed on 20 July 2022).
26. DrivAer Model. Available online: <https://www.epc.ed.tum.de/en/aer/research-groups/automotive/drivaer/> (accessed on 31 June 2022).
27. Ashton, N.; Revell, A. *Comparison of RANS and DES Methods for the DrivAer Automotive Body*; SAE Technical Paper 2015-01-1538; SAE International: Warrendale, PA, USA, 2015. [[CrossRef](#)]
28. Lanfrit, M. Best Practice Guidelines for Handling Automotive External Aerodynamics with FLUENT Version 1.2. 2005. Available online: https://www.southampton.ac.uk/~{nwb}/lectures/GoodPracticeCFD/Articles/Ext_Aero_Best_Practice_Ver1_2.pdf (accessed on 20 July 2022).

29. Piechna, J.R.; Kurec, K.; Broniszewski, J.; Remer, M.; Piechna, A.; Kamieniecki, K.; Bibik, P. Influence of the Car Movable Aerodynamic Elements on Fast Road Car Cornering. *Energies* **2022**, *15*, 689. [[CrossRef](#)]
30. Tudruj, S.; Piechna, J. New model of the simulation of the airbag operation in the case of the out-of-position occupant—the comparison with existing models. *Arch. Mech. Eng.* **2003**, *2*, 201–223.
31. Tudruj, S.; Piechna, J.; Dziewoński, T. *Influence of the Outside Inertia Effect on Airbag Deployment*; IRCOBI: Gratz, Austria, 2004; pp. 339–340.
32. Tudruj, S.; Piechna, J. Numerical Analysis of the Possibility of Using an External Air Bag to Protect a Small Urban Vehicle during a Collision. *Arch. Mech. Eng.* **2012**, *59*, 257–281. [[CrossRef](#)]
33. Harper, C. *Handbook of Plastics, Elastomers, and Composites*; McGraw-Hill Education: New York, NY, USA, 2002.